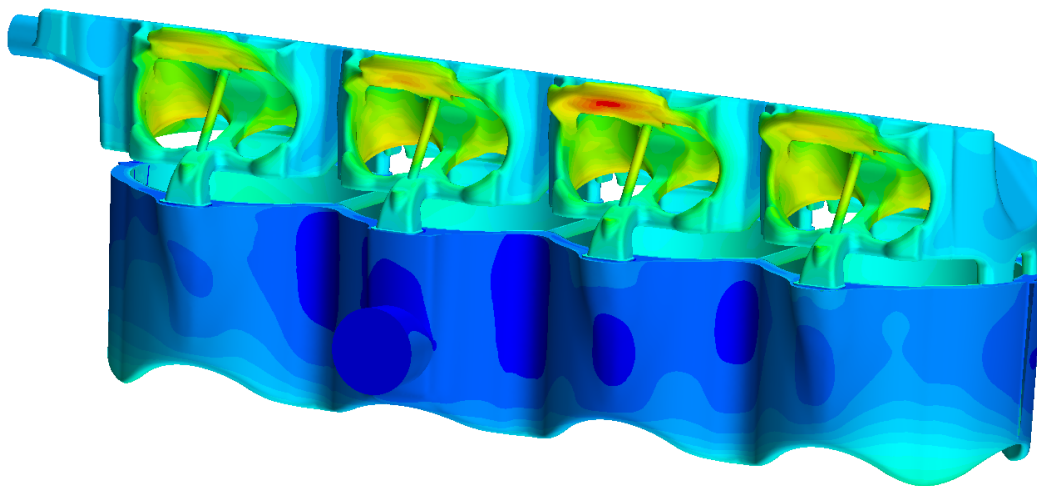


CHALMERS



Numerical modeling of subcooled nucleate flow boiling in engine cooling systems

Master's thesis in the Applied Mechanics programme

FREDRIK ÖHRBY

Department of Applied Mechanics
Division of Fluid Dynamics
CHALMERS UNIVERSITY OF TECHNOLOGY
Göteborg, Sweden 2014
Master's thesis 2014:31

MASTER'S THESIS IN THE APPLIED MECHANICS PROGRAMME

Numerical modeling of subcooled nucleate flow boiling in engine cooling
systems

FREDRIK ÖHRBY

Department of Applied Mechanics
Division of Fluid Dynamics
CHALMERS UNIVERSITY OF TECHNOLOGY
Göteborg, Sweden 2014

Numerical modeling of subcooled nucleate flow boiling in engine cooling systems
FREDRIK ÖHRBY

© FREDRIK ÖHRBY, 2014

Master's thesis 2014:31
ISSN 1652-8557
Department of Applied Mechanics
Division of Fluid Dynamics
Chalmers University of Technology
SE-412 96 Göteborg
Sweden
Telephone: +46 (0)31-772 1000

Cover:

Estimated temperature distribution at the fluid-solid interface of an engine cooling jacket using the Chen correlation.

Chalmers Reproservice
Göteborg, Sweden 2014

Numerical modeling of subcooled nucleate flow boiling in engine cooling systems
Master's thesis in the Applied Mechanics programme
FREDRIK ÖHRBY
Department of Applied Mechanics
Division of Fluid Dynamics
Chalmers University of Technology

ABSTRACT

The demands for high power and low emissions put focus on energy efficiency when developing new engines. An important part is the engine cooling system, which cools the engine structure below damaging temperatures. For high temperatures in the cooling system there is a risk that boiling occurs and while the initial nucleate boiling enhances the cooling effect the subsequent film boiling decreases the heat transfer drastically. Volvo Cars therefore aims to develop a method that can predict the presence of boiling and estimate the heat transfer effects. As a first step, one-dimensional boiling models and correlations in combination with three-dimensional Computational Fluid Dynamics (CFD) analysis are investigated. A set of chosen models have been evaluated in Matlab and in the commercial CFD code Star-CCM+. An expression to predict the presence of boiling has successfully been implemented into the software and when applied to an engine cooling jacket, boiling is predicted to occur in those areas where it is expected. The heat transfer effects are estimated using the Chen correlation [1, 2] together with the Dry-spot model [3, 4, 5] with promising results but convergence issues appear for the Dry-spot model at high wall temperatures. A method has also been created to indicate the presence of critical film boiling and when applied to the engine cooling jacket, film boiling is indicated mainly in the cylinder head around the exhaust ports. Before including the developed methods in the standard analysis of the engine cooling jacket, further work is needed to improve and validate the estimations of the heat transfer and to solve the convergence issues.

Keywords: Numerical modeling, boiling, heat transfer, engine cooling, subcooled nucleate boiling, Chen correlation, Dry-spot model, CFD

SAMMANFATTNING

Kraven på hög effekt och låga utsläpp sätter fokus på energieffektivisering vid utveckling av nya motorer. En viktig del är motorns kylsystem som kyler motorblocket och ser till att för höga temperaturer inte uppnås. Vid höga temperaturer i kylsystemet finns risk för att kylmediet börjar koka och medan den inledande kärnkokningen förbättrar kylningen, försämrar den efterföljande filmkokningen värmeöverföringen avsevärt. Volvo Cars vill med anledning av detta utveckla en metod för att prediktera om kokning sker och för att uppskatta kokningens effekt på värmeöverföringen i deras kylmantlar. Som ett första steg har endimensionella kokmodeller och korrelationer i kombination med tredimensionell CFD-analys undersökts. Utvalda modeller har utvärderats i Matlab och i den kommersiella CFD-programvaran Star-CCM+. Ett uttryck för att prediktera om kokning sker har implementerats och visar på kokning i de förväntade områdena för en kylmantel. En kombination av Chen korrelationen [1, 2] och Dry-spot modellen [3, 4, 5] används för att undersöka hur värmeöverföringen påverkas av kokningen. Resultaten är lovande men konvergensproblem uppkommer vid användandet av Dry-spot modellen för höga väggtemperaturer. Utöver detta har en metod utvecklats för att uppskatta om det finns risk för filmkokning. När metoden används för kylmanteln indikeras filmkokning främst i cylinderhuvudet kring avgasportarna. Ytterligare arbete krävs innan de utvecklade metoderna kan inkluderas i standardanalyserna för kylmanteln. Framförallt måste konvergensproblemen lösas och metoden för att uppskatta kokningens effekt på värmeöverföringen förbättras och valideras.

Nyckelord: Numerisk modellering, kokning, värmeöverföring, motorkylning, kylmantel

PREFACE

In this study, the possibilities of modeling boiling heat transfer in engine cooling systems using one-dimensional correlations and models have been investigated. The work has been carried out during January to June in 2014 and is part of the master programme Applied Mechanics. The work is a collaboration with Volvo Cars and the division of Fluid Dynamics within the department of Applied mechanics, Chalmers University of Technology, Sweden.

This master thesis has been executed with Associate Professor Srdjan Sasic as examiner and Sofia Ebermark and Stefan Eriksson from Volvo Cars as supervisors. Thank you for making this thesis work possible. A special thank you to Volvo Cars for supplying software and workplace during these months and I would also like to thank Martin Hübert for his valuable help with Star-CCM+. Finally, I am most grateful for the help from Anna Broberg who continuously supported me in my work.

Gothenburg, June 2014

Fredrik Öhrby

CONTENTS

Abstract	i
Sammanfattning	ii
Preface	iii
Contents	v
Nomenclature	vii
1 Introduction	1
1.1 Aim	1
1.2 Method	1
1.3 Limitations	1
2 Theory	3
2.1 Heat transfer in engine cooling systems	3
2.2 Heat transfer during subcooled flow boiling	3
2.2.1 Heat transfer mechanisms in the nucleate boiling regime	6
2.3 Different approaches of modeling boiling heat transfer	6
2.4 One dimensional modeling of nucleate boiling heat transfer	7
2.5 Correlations applied to engine cooling jackets	8
2.6 Evaluated models and correlations	8
2.6.1 Single-phase forced convection	8
2.6.2 Onset of Nucleate Boiling (ONB)	9
2.6.3 The Chen correlation	10
2.6.4 The Dry-spot model	11
2.6.5 Film boiling	13
3 Method	15
3.1 Properties of vapor and coolant mixture	15
3.2 Modeling setup	15
3.3 Simulations in Matlab	16
3.4 Simulations in Star-CCM+	17
3.4.1 Implementation of models	17
3.4.2 Test case	19
3.4.3 Engine cooling jacket	22
4 Results	25
4.1 Simulations in Matlab	25
4.1.1 Effects of velocity	26
4.1.2 Effects of suppression factor	28
4.1.3 Effects of inlet subcooling	29
4.1.4 Trends of bubble departure diameter and active nucleation site density	31
4.2 Simulations in Star-CCM+	33
4.2.1 Test case	33
4.2.2 Engine cooling jacket	39
5 Discussion	43
6 Conclusions	45
7 Further work	47
References	49

NOMENCLATURE

ROMAN SYMBOLS

Symbol	Description
a	Width of duct [m]
A	Area [m^2]
b	Height of duct [m]
c_p	Specific heat capacity [$J/(kg K)$]
d	Diameter [m]
d_h	Hydraulic diameter [m]
d_{av}	Time-averaged bubble diameter [m]
d_d	Bubble departure diameter [m]
d_{dF}	Fritz bubble departure diameter [m]
F	Multiplier for saturated flow conditions
g	Gravity constant [m/s^2]
h	Heat transfer coefficient [$W/(m^2 K)$]
i	Enthalpy [J/kg]
i_{lv}	Latent heat of vaporization [J/kg]
k	Thermal conductivity [$W/(m K)$]
\dot{m}	Mass flow rate [kg/s]
n	Number of active nucleation sites
n_c	Critical number of active nucleation sites
N	Active nucleation site density [$1/m^2$]
\bar{N}	Average active nucleation site density [$1/m^2$]
\bar{N}_d	Average number density of dry-spots [$1/m^2$]
\bar{N}'	Dimensionless active nucleation site density
p	Pressure [Pa]
P	Probability function
q	Heat flux [W/m^2]
R_c	Critical cavity radius [m]
R'_c	Dimensionless cavity radius
R	Specific gas constant [$J/(kg K)$]
S	Nucleate boiling suppression factor
T	Temperature [K]
T^+	Dimensionless temperature
ΔT	Temperature difference [K]
ΔT_e	Effective superheat [K]
ΔT_{sat}	Wall superheat [K]
ΔT_{sub}	Subcooling [K]
u_τ	Characteristic friction velocity [m/s]
V	Velocity [m/s]
W	Wetted perimeter [m]
x	Equilibrium quality
X_{tt}	Lockhart-Martinelli parameter
y_c	Normal distance of near wall cell [m]
y^+	Dimensionless wall distance

GREEK SYMBOLS

Symbol	Description
Γ	Fraction of dry area
θ	Bubble contact angle [$^\circ$]
μ	Dynamic viscosity [$Pa s$]
ν	Kinematic viscosity [m^2/s]
ρ	Density [kg/m^3]
σ	Surface tension [N/m]

SUBSCRIPTS

Symbol	Description
b	Bulk liquid
c	Cell adjacent to wall
fc	Forced convection
l	Liquid
nb	Nucleate boiling
ONB	Onset of Nucleate Boiling
ref	Reference quantity
sat	Saturation condition
sub	Subcooled condition
tp	Two-phase
v	Vapor
w	Wall

ABBREVIATIONS

CAE	Computer Aided Engineering
CFD	Computational Fluid Dynamics
CHF	Critical Heat Flux
DNB	Departure from Nucleate Boiling
FDB	Fully Developed nucleate Boiling
ONB	Onset of Nucleate Boiling
OSV	Onset of Significant Voids
PDB	Partially Developed nucleate Boiling
1D	One-Dimensional
3D	Three-Dimensional

1 Introduction

Passenger cars are central in everyday life in most countries. They offer a convenient way for transportation and are seen by many as a necessity. However, the increased awareness of the global climate change have put focus on the environmental effects of internal combustion engines, which have resulted in continuously increasing legislative demands on fuel consumption and emissions. Simultaneously, there is a consumer demand for high power and affordable prices, posing a major challenge for the automotive industry. A high energy efficiency is crucial to meet the increased demands and the process of engine cooling is an important part in achieving this. Often it is necessary to operate the engine at very high cooling temperatures, close to the saturation temperature of the coolant, and higher temperatures implies a larger risk that boiling can occur in the engine cooling jacket. While the initial nucleate boiling enhances the heat transfer between the coolant and the engine structure, which gives a more efficient cooling, the subsequent film boiling reduces the heat transfer drastically [6]. If the boiling can be controlled within the nucleate boiling regime it can be favourable to operate the cooling system at higher temperatures but if film boiling is developed, the high temperatures can cause break down of the engine structure. It is therefore necessary to be able to predict when and where boiling is prone to occur in the engine cooling jacket and if the boiling is in the nucleate regime or not.

Previous research has shown that it is possible to predict boiling with one-dimensional (1D) models and correlations. The conditions in an engine cooling jacket implies that it might be reasonable to assume that the boiling that occurs can be considered as subcooled flow boiling. This means that the bulk flow temperature is lower than the saturation temperature of the liquid and that the vapor bubbles that depart from the wall are rapidly consumed by the bulk flow. The vapor bubbles will therefore have little or no effect on the flow and the main area of interest is the heat transfer at the walls. This implies that 1D models is suitable to estimate the effects of boiling [7, 8].

Volvo Cars is continuously working on improving their modeling methods and numerical simulations are an important part in the development of new engines. A well-functioning engine cooling jacket is vital to achieve high energy efficiency and safe operation of the engine. To improve the understanding of the heat transfer in the cooling jacket, Volvo Cars aims at including boiling in their standard CAE (Computer Aided Engineering) analysis. To learn more about the subject it is of interest to investigate the possibilities of using 1D boiling heat transfer models in combination with the standard three-dimensional (3D) Computational Fluid Dynamics (CFD) analysis.

1.1 Aim

The thesis work aims at finding a method to model boiling heat transfer in engine cooling jackets that are part of the Volvo Cars engine design. The main purpose is to predict the presence of boiling, describe how the heat transfer is affected by boiling and predict the limit when boiling starts to have a negative impact on the heat transfer. The focus is on 1D boiling correlations and models used together with 3D CFD analysis. This thesis is a first step towards including boiling in the standard CAE analysis of engine cooling jackets at Volvo Cars.

1.2 Method

The mechanisms and phenomena of boiling have been evaluated as well as available models and methods. Suitable models are chosen and implemented in Matlab for an initial 1D analysis and parameter study. To study the models in 3D they are also implemented in the commercial CFD software Star-CCM+. A test case is constructed to evaluate the boiling models on a simple geometry and the models are applied on the more complex geometry of an engine cooling jacket.

1.3 Limitations

No new models for boiling heat transfer has been developed. The thesis work only considers models already established and available in the literature. Existing set-up for CFD simulations of engine cooling jackets at Volvo Cars are used for the simulations unless the boiling models require otherwise. For example, mesh or

choice of turbulence models are not investigated. In this thesis only 1D boiling models and correlations are considered and the boiling is assumed to be subcooled flow boiling. The work focus on the convective part and the initial nucleate boiling part of the heat transfer. The subsequent film boiling is included but not investigated further.

2 Theory

2.1 Heat transfer in engine cooling systems

Internal combustion engines normally operate at fairly high temperatures. This is advantageous since the combustion process is less efficient when the engine is cold and more pollution is then emitted. At lower temperatures the components in the engine also wear out faster. However, too high temperatures can damage the engine structure and therefore a cooling system is needed to transport excess heat away from the engine to keep the temperatures at a certain level. A simplified description of a typical engine cooling system in a modern car is illustrated in figure 2.1. The engine cooling jacket consists of a complex duct geometry integrated in the cylinder head and block. A coolant liquid flows through the cooling jacket and transports heat away from the hot walls. The flow into the cooling jacket is regulated by a pump and the liquid is cooled in the radiator, which exchanges heat with the surrounding air that is blown through it. The liquid that flows from the cooling jacket passes by a thermostat that regulates the flow. If the engine is running at operating conditions the thermostat is opened and the liquid flows to the radiator to be cooled. But if the engine is cold the thermostat closes and the liquid is sent back to the pump. In this way it is possible to allow the engine to heat up quickly. Apart from the outlet to the thermostat there is a separate circuit to the heating system of the cabin [9].

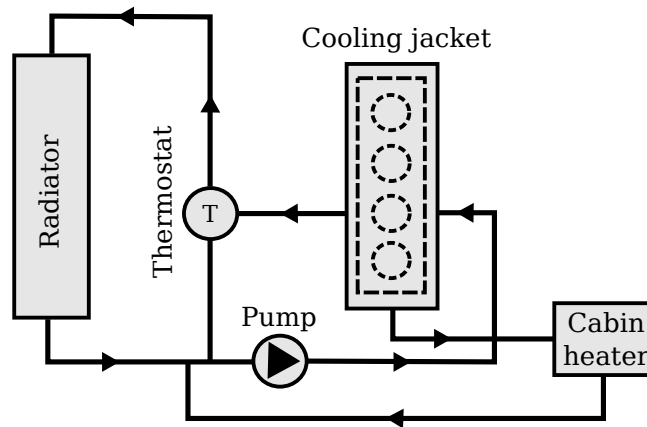


Figure 2.1: *Illustration of a simplified circuit of an engine cooling system.*

The bulk temperature of the coolant liquid in the engine cooling jacket is normally controlled below the saturation temperature and it is therefore applicable to consider the boiling that occurs at the wall to be within the subcooled nucleate boiling regime (section 2.2). Depending on flow situation, wall temperature and geometry it is possible that more developed boiling occurs locally and in worst case film boiling is developed. Film boiling severely decreases the heat transfer capacity and it is of great importance to be able to accurately predict and model the heat transfer to prevent the risk of overheating, which may result in damage to the structure of the engine. The cooling jacket includes flow of various regimes where different heat and flow mechanisms are present. In order to model the boiling heat transfer accurately, separate models are normally needed to describe and estimate the heat transfer depending on what phenomenon that is present [7].

2.2 Heat transfer during subcooled flow boiling

Boiling is a heat transfer process where liquid change phase to vapor and can occur on heated solid surfaces or in superheated liquid regions next to the heated surface. Boiling differs from evaporation in that matter that evaporation is a phase change over an already existing liquid-vapor interface, whether boiling also creates these interfaces since vapor bubbles are formed in cavities on the surface [7]. The boiling processes are characterized into pool boiling if the liquid is standing still or into flow boiling when there is a flow field present [6]. When

considering the application of an engine cooling system the boiling process will mainly be that of flow boiling.

When working with boiling heat transfer, temperatures are often related to the saturation temperature of the liquid. A liquid is said to be subcooled if the bulk temperature is below the saturation temperature of the liquid and the temperature difference is denoted as ΔT_{sub} . It is also common to use the notion superheated when the temperature is higher than the saturation temperature. The so called wall superheat is the difference between the wall temperature and the saturation temperature and is denoted ΔT_{sat} [2].

$$\begin{aligned}\Delta T_{sub} &= T_{sat} - T_l \\ \Delta T_{sat} &= T_w - T_{sat}\end{aligned}\tag{2.1}$$

The boiling process for a subcooled channel flow, where the fluid is heated at the walls, develops through a number of flow regimes with different characteristics. The different regimes are illustrated for a channel flow with heated walls in figure 2.2. For the first region, before boiling is present, the heat transfer mechanism is single-phase forced convection from the solid surface to the liquid. If the wall temperature is increased a certain amount over the saturation temperature of the liquid, isolated vapor bubbles will form at cavities and irregularities at the wall. This point is called the Onset of Nucleate Boiling (ONB). Slightly after the ONB, the bubbles are still small and attached to the wall. When the wall superheat increases further the bubbles grow larger and start to move along the wall as the bulk temperature is increased. When the superheat is increased some more the bubbles start to depart from the wall. This is called the Onset of Significant Voids (OSV) and the flow can after this point be considered as two-phase. With further increase in superheat, bubbles grow and lift off from the surface more rapidly and start to merge into jets leaving the surface. The boiling is then considered as Fully Developed nucleate Boiling (FDB) [6].

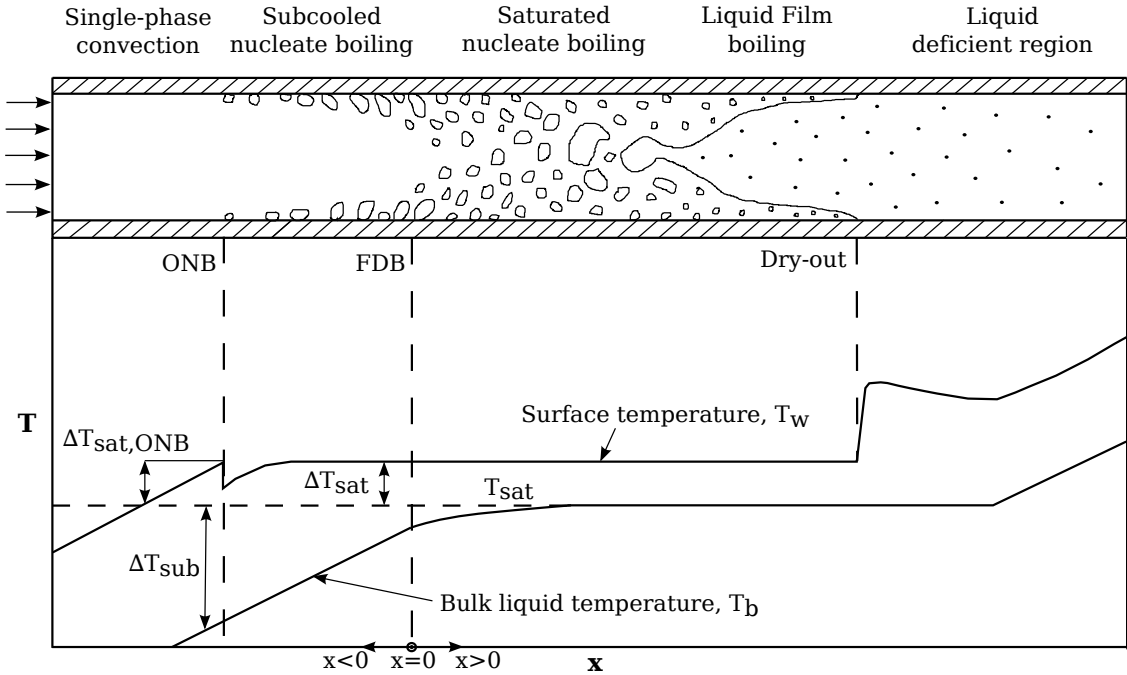


Figure 2.2: Schematic representation of the boiling regimes during subcooled flow boiling.

The part of the process between the ONB and the transition to FDB is called Partial Developed nucleate Boiling (PDB). The heat transfer in this region is increased due to the nucleate boiling and is at this state dominated by the forced convection from the motion of the bulk flow and a contribution associated to the nucleate boiling. Since the heat transfer is increased at the ONB the temperature decrease some which explain that a certain amount of wall superheat is needed to be able to initiate the boiling process. As the wall superheat is increased

more and the boiling develops further, the effects from the nucleate boiling in the PDB regime become more pronounced and the influence of the forced convection diminishes as the transition to FDB is approached. The heat transfer during FDB can be considered independent of the convection [6].

The vapor bubbles that depart from the surfaces at the point of OSV are at the saturation temperature. Since the bulk liquid still is at subcooled conditions, a state of thermodynamic non-equilibrium is present between the vapor and the liquid where the temperature of the liquid falls below the temperature of the equilibrium subcooled liquid. When more heat is added, thermodynamic equilibrium is reached which defines the condition for saturated flow boiling [6]. The equilibrium state of the liquid can be expressed as a so called equilibrium quality defined as

$$x = \frac{\dot{i}_l - \dot{i}_{l,sat}}{\dot{i}_{lv}} \quad (2.2)$$

The equilibrium quality, sometimes also called vapor quality, takes a negative value in the subcooled nucleate boiling regime and starts at zero in the shift from subcooled to saturated nucleate boiling. Saturated nucleate flow boiling is then defined as the regime where the wall temperature exceeds the local saturation temperature of the liquid and where the equilibrium thermodynamic quality is between 0 and 1 [6].

When more vapor is generated in the nucleate boiling regime, bubbles start to coalesce and the flow pattern can change into a slug or plug flow. At even higher equilibrium qualities an annular flow pattern can form with a continuous vapor core and a surrounding liquid film covering the surfaces. The vapor is at this stage produced through evaporation between the liquid-vapor interface and the heat transfer mechanism changes from nucleate boiling to convective heat transfer through the film. Liquid droplets also leave the film and mix in the vapor phase and when the whole liquid film is depleted through evaporation, the point of so called dry-out is reached. The small liquid droplets that are left in the vapor phase will continue to evaporate until a dry single-phase vapor flow is present. The part of the flow pattern between dry-out and single-phase vapor flow is called the liquid deficient region [6, 2].

At the point of dry-out the depletion of the liquid layer leads to a significant decrease in heat transfer at the surface which will result in an increase in wall temperature. But apart from the dry-out condition, a similar decrease in heat transfer can also occur at lower vapor qualities during the subcooled or saturated nucleate boiling regimes. This condition is achieved at high heat fluxes when rapid nucleation of bubbles result in formation of dry areas that start to cover more and more of the surface. Finally, a vapor film separates the liquid from the surface and film boiling has been initiated. This cause a drastic reduction in heat transfer since the vapor has a much lower thermal conductivity than the liquid. The condition is referred to as Departure from Nucleate Boiling (DNB) where the point of maximum heat flux is called the Critical Heat Flux (CHF) [2, 10].

By controlling the temperature at a wall and monitoring the wall heat flux it is possible to generate a boiling curve where the characteristic changes in wall heat flux with temperature can be studied for the different boiling regimes. A typical boiling curve is presented in figure 2.3. The first part of the curve (A-B) is the region before boiling is present and convection is the dominant heat transfer mechanism. Point B' indicate the ONB point which is followed by a temperature drop to point B'' because of the increased heat transfer due to nucleation of vapor bubbles. Then the PDB region follows (B''-C) which develops into FDB (C-D). Point E represent the CHF during nucleate boiling conditions when a thin film of vapor start to form on the surfaces. During stable conditions when the temperature at the wall is controlled, the curve continues into the transition region (E-F) and later fully developed film boiling (F-G). The dotted arrow (E-G) illustrate the fast jump in temperature that is achieved if the heat flux is controlled instead of the wall temperature [6].

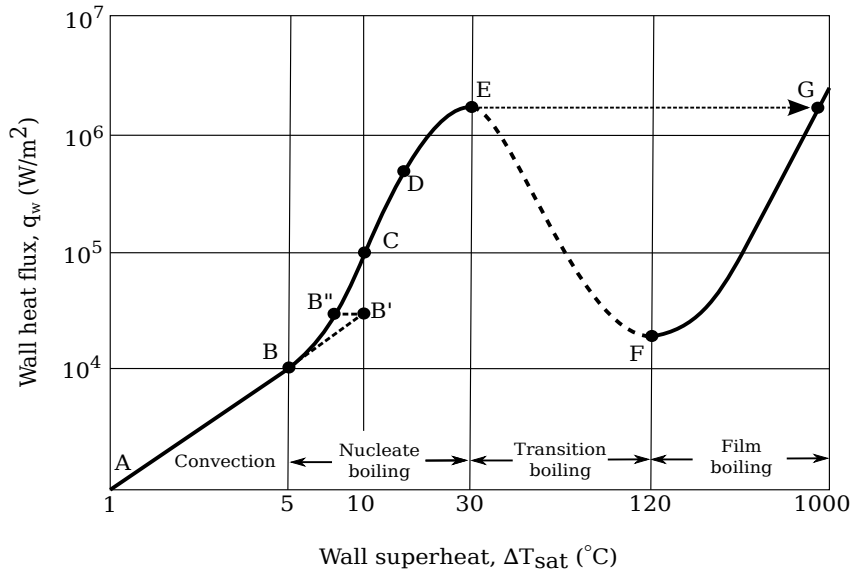


Figure 2.3: A typical boiling curve showing the different boiling regimes.

2.2.1 Heat transfer mechanisms in the nucleate boiling regime

Regarding the heat transfer effects in the nucleate boiling regime the mechanisms of nucleate boiling are usually considered to consist of three main parts [6]:

- Transient conduction
- Enhanced convection
- Microlayer evaporation

Transient conduction includes the process where liquid flows from the bulk liquid to the wall after a bubble moves away from the surface. The liquid is heated through conduction from the solid wall and later transferred back to the bulk liquid when vapor bubbles grow and depart from the surface. The heated liquid layer also contributes to the process of evaporation at the interfaces of the bubbles. Enhanced convection is an effect of several mechanisms. Convective currents and flow patterns are created when bubble columns depart from a wall surface, the wake flow behind a vapor bubble contribute to the convection of heat from the wall and growth and collapse of vapor bubbles near the wall give rise to micro convection by random liquid motion [11]. Microlayer evaporation refers to evaporation of the thin microlayer of liquid that is left below a growing bubble. The effect is most significant for the heat transfer at higher heat fluxes. It is these different mechanisms that the boiling heat transfer models aim to describe or mimic [6].

2.3 Different approaches of modeling boiling heat transfer

There are several approaches and methods that can be used to model the two-phase flow phenomenon of boiling with CFD. Many of the approaches are focused on predicting the presence of boiling and the thermal effects at the wall while other approaches also try to model the whole two-phase flow phenomenon more thoroughly with interactions between the phases.

One common approach is the use of 1D models and correlations to describe the heat transfer effects by modifying the heat fluxes at the walls. The approach has been used in single-phase flow simulations as well as in simulations that adopt multiphase flow frameworks. When using the models and correlations with single-phase flow simulations, the thermal effects at the walls are the only effects of boiling that are taken into account.

Because of the use of single-phase flow models, the two-phase effects of the flow are not modeled and the flow can therefore not be described accurately when there is an increased fraction of vapor present. This is also the main disadvantage of the approach since energy added will directly give an increase in temperature but not result in any phase change. The models and correlations are generally developed for specific cases and have potential to give accurate predictions of the wall temperature as long as they are used for the conditions that they were developed for. The boiling correlation or model is in this case normally used when a certain ONB criterion is satisfied [7, 12].

An extension to this first approach is to use a homogeneous flow model where both the liquid and vapor phases are represented as a mixture. The vapor bubbles and the liquid are in this case assumed to be perfectly mixed and an additional equation for the vapor fraction is introduced to estimate the concentration of vapor. The governing equations are therefore still single-phase but with the addition of the vapor equation. The advantage of using this approach is that the changes in density due to the phase change of the liquid can be taken into account without solving two sets of governing equations for the liquid and vapor phases. The boiling is still accounted for similarly as when using only the single-phase flow models with 1D models and correlations [6, 13, 14].

A third possibility is to use a multiphase flow model where the vapor and liquid phases are solved separately using different governing equations for each phase. The mass, momentum and energy transfer over the interfaces between the phases are described using additional models. A key aspect when using these models is how to handle the different sizes of the vapor bubbles and the interfaces between the bubbles and the liquid. In the so called Eulerian-Eulerian multiphase framework the bubbles are assumed to be of a certain size and the computational mesh cell size needs to be larger than the bubbles. This means that the interfaces between the bubbles are not resolved completely and the interactions between the phases are handled based on estimations of bubble size and number density. To be able to predict the interfaces when the bubbles grow larger than the cell size it is possible to combine the framework with an interface treatment model such as the Volume of Fluid model [6].

2.4 One dimensional modeling of nucleate boiling heat transfer

There is a wide range of 1D models and correlations that have been developed with the aim of predicting heat transfer during subcooled flow boiling conditions but none of them have been accepted as a standard. Since the models are 1D, they often use bulk properties of the flow that are averaged over a cross-sectional area normal to the mean flow. The different models can essentially be divided into empirical correlations and mechanistic models. The empirical correlations are usually derived through analysis of experimental results while the more mechanistic models aim to describe the physics of the boiling heat transfer process or sub-processes theoretically. The empirical correlations can further be divided into correlations used to estimate the wall heat flux and correlations that try to estimate the partitioning of the wall heat flux, i.e. what components the heat flux consists of [12].

The empirical correlations for wall heat flux are correlations built from curve fittings of experimental data with the aim to predict the total heat flux boiling curve, including the single-phase convection region, the partial nucleate boiling region and the fully developed boiling region. Because the correlations do not model the heat transfer mechanisms of the boiling, they are not able to give any information about the partitioning of the wall heat flux. For example it can in some applications be important to know how much of the heat flux that is used to heat the bulk liquid and how much that is used for vapor generation. This is the aim of the empirical correlations for partitioning of the wall heat flux [12]. These models try to determine the components of the heat flux from relevant heat transfer mechanisms. But since the components are not calculated independently of each other, the models are not able to predict the total wall heat flux by themselves. A disadvantage of the empirical correlations is that it can turn out to be significant differences between predictions and experimental data if the correlations are used for other conditions than they were developed for [15].

The mechanistic models try to describe the wall heat transfer by breaking down the mechanisms of the heat transfer and independently describe them (section 2.2.1). The models can therefore be used to predict the total wall heat flux as well as the partitioning. However, the present models are often developed for certain cases and have very limited usability outside of this range. The models are also complex since the mechanisms

that are modelled need additional sub-models or correlations [12]. Because the mechanistic models have not yet been used to predict the nucleate boiling heat flux successfully for wider applications and that they often are more complex to implement, empirical correlations have mostly been used up to now [6, 15].

2.5 Correlations applied to engine cooling jackets

There are a few studies in the literature that have carried out CFD simulations with the focus on boiling heat transfer in engine cooling jackets. The studies have almost without exception used the boiling heat transfer correlations of Chen [1] and Rohsenow [16] where the correlation of Chen has been most popular. Both models use a super-positioning approach where the heat flux during nucleate boiling is assumed to consist of a convective and a nucleate boiling component with some modifications.

In the PhD thesis by Robinson [8] the correlation of Chen was studied and modified with focus on the convective part of the correlation. The model was applied to a simplified test case aimed at representing the geometry of an engine cooling jacket and later also applied to the real case. The results have been used by other researchers for validation purposes. Several other researchers have also applied the Chen correlation to the application of an engine cooling jacket, for instance Cardone et al [17] and Lee [18]. Punekar and Das [13] have used the Chen correlation together with a homogeneous mixture model where a second equation for the volume fraction of vapor is computed. This approach was also used by Bo [14] who performed simulations for an engine cooling jacket using the Rohsenow correlation. Campbell et al [19] applied the Chen and Rohsenow correlations to a test case aimed at representing an engine cooling system where the Chen approach gave the best representative results. Dong et al [20] also analyzed results for a test case where the Chen correlation was compared with results from a combined approach where the Rohsenow correlation was used together with an interpolation expression for the partial nucleate boiling regime by Bergles and Rohsenow [21]. The results were also compared with the so called Boundary Departure Lift-off (BDL) model [22] which is a further modification of the Chen approach aimed at making it less dependent on geometry. The BDL model and the combined Rohsenow approach gave the best results for the used setup.

2.6 Evaluated models and correlations

There are several different 1D correlations and models available in the literature to describe the boiling heat transfer as presented in section 2.4, many more than those applied to engine cooling systems described in section 2.5. Different numerical methods are used, for instance additive, asymptotic and power law approaches. Some are more complex than others but common for most of the models are that they often are developed for very specific conditions and there is no standard approach to model boiling since the majority of the correlations and models in the literature have not been used for wider applications [7, 12]. The models and correlations used in this thesis work are described further in the following sections.

2.6.1 Single-phase forced convection

Before the ONB in subcooled flows the heat transfer is dominated by forced convection, which is also an important part in the beginning of nucleate boiling. Convective heat transfer can be computed through Newton's law of cooling defined as

$$q_{fc} = h_{fc}(T_w - T_{ref}) \quad (2.3)$$

where the surface heat flux due to convection q_{fc} is computed related to a convective heat transfer coefficient h_{fc} , the temperature of the surface T_w and a certain characteristic reference temperature T_{ref} of the fluid. To estimate the heat transfer coefficient, the widely used Dittus-Boelter correlation for convective heat transfer in pipe flows can be used. The correlation is given as a Nusselt number relationship, as presented in the following equation, and is applicable to fully developed turbulent and thermal flows in smooth channels [23]. Because the Dittus-Boelter correlation is based on the properties of the bulk flow, it is the bulk flow temperature that should be used in Newton's law of cooling as the reference temperature when the boundary heat flux is computed.

$$Nu_d = 0.023Re_d^{0.8}Pr^{0.4} \quad (2.4)$$

The fluid properties is evaluated at the mean bulk temperature and the dimensionless numbers are defined as

$$Nu_d = \frac{hd}{k}, \quad Re_d = \frac{\rho V d}{\mu}, \quad Pr = \frac{\mu c_p}{k} \quad (2.5)$$

By reordering equation 2.4 the heat transfer coefficient for forced convection h_{fc} can be expressed as

$$h_{fc} = 0.023 Re_d^{0.8} Pr^{0.4} \frac{k}{d} \quad (2.6)$$

For a channel flow the characteristic length d is usually defined as the diameter of the channel. In the case of a channel with a non-circular cross-section the diameter can be expressed as an equivalent, or also called hydraulic, diameter defined as [24]

$$d_h = \frac{4A}{W} \quad (2.7)$$

where A is the cross-sectional area and W the wetted perimeter of the cross-section. For a rectangular channel completely filled with a fluid, the hydraulic diameter is defined as below where a and b is the width and height of the channel respectively.

$$d_h = \frac{4ab}{2a + 2b} \quad (2.8)$$

In Star-CCM+ the contribution to the boundary heat flux due to convection is computed locally based on the standard wall functions and with the temperature of the near wall cell T_c as the reference temperature. The heat transfer coefficients are then computed as

$$h = \frac{\rho_l(y_c) c_{p,l}(y_c) u_\tau}{T^+(y^+(y_c))} \quad (2.9)$$

where u_τ is the friction velocity, a velocity scale based on the wall shear stress, T^+ is the dimensionless temperature, y_c the normal distance of the near wall cell and y^+ is the dimensionless wall distance computed as

$$y^+ = \frac{u_\tau y_c}{\nu_l} \quad (2.10)$$

The convective heat transfer coefficient is always computed internally in Star-CCM+ as in equation 2.9 but it is possible convert it to other forms by post-processing, for example if the heat transfer coefficients should be presented related to another reference temperature than T_c [25].

2.6.2 Onset of Nucleate Boiling (ONB)

In order to predict when nucleate boiling starts to occur a condition is needed for when the heat transfer changes from single-phase to two-phase heat transfer. The nucleate boiling during subcooled flow conditions is initiated at nucleation cavities on the heated surfaces. The cavities trap vapor and bubbles are formed when a certain amount of superheat is reached. The amount of superheat that is needed to activate the cavities depend on many different factors, for example [6]

- Cavity size
- Cavity shape
- Temperature profile in the near wall region
- Fluid properties (such as surface tension and bubble contact angles against the surface)

A common approach to establish a condition for the ONB is that of Hsu [26]. He postulated that for a vapor nucleus to grow into a bubble the temperature at the tip of the bubble needs to be equal or larger than the saturation temperature of the liquid corresponding to the pressure inside the bubble. By assuming a linear temperature drop in the thermal boundary layer, truncated bubbles with 90° bubble contact angle and a wide range of cavities of all sizes Hsu came up with an expression to estimate the wall superheat at onset of nucleate boiling as [6]

$$\Delta T_{sat,ONB} = \frac{4\sigma T_{sat} h_l}{k_l i_{lv} \rho_{lv}} \left[1 + \sqrt{1 + \frac{k_l i_{lv} \rho_{lv} \Delta T_{sub}}{2\sigma T_{sat} h_l}} \right] \quad (2.11)$$

where h_l is the single-phase convective heat transfer coefficient and ρ_{lv} the density at the saturation temperature. The bubble contact angle of the nucleating vapor bubbles are the angle between the bubble and the surface as defined in figure 2.4. The condition of Hsu is used widely in practical applications and has proven to give reasonable estimates of ONB [6]. Since it is assumed that a wide range of active cavities of all sizes are present on the surface the estimated superheat is equal to the minimum wall superheat at nucleation. However, if the range of active cavity sizes available on the surface is reduced, the ONB superheat will be underestimated using equation 2.11. This can for example be the case if the cavities are filled with liquid or if the surface is very smooth [27].

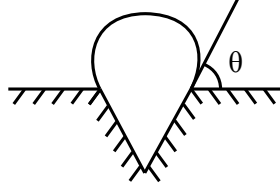


Figure 2.4: The definition of the bubble contact angle θ for a bubble growing at an active nucleation site.

2.6.3 The Chen correlation

The Chen correlation [1] is a widely used correlation to estimate the wall heat transfer coefficients in flow boiling. One reason for this is probably the fact that no tests or experiments have to be performed to determine empirical constants. The Chen correlation was originally developed for vertical channel flow for pure liquids with axisymmetric heating but has in several studies been applied to other systems, for example the application of the cooling systems in internal combustion engines as described in section 2.5. The correlation was also primarily developed for saturated flow boiling but has been extended for use in the subcooled flow boiling region [2]. The correlation uses an additive approach to describe the components of the heat flux consisting of one part from forced convection q_{fc} and one part from the contribution of nucleate boiling q_{nb} as expressed by the following equation.

$$q = q_{fc} + q_{nb} = h_{fc}(T_w - T_b) + h_{nb}(T_w - T_{sat}) \quad (2.12)$$

Here T_b is the temperature of the bulk liquid. The nucleate boiling heat transfer coefficient h_{nb} is derived from a dimensionless Nusselt number relationship presented by Forster and Zuber [28] and the final equation is given as [2]

$$h_{nb} = 0.00122 \left(\frac{k_l^{0.79} c_{p,l}^{0.45} \rho_l^{0.49}}{\sigma^{0.5} \mu_l^{0.29} \rho_{lv}^{0.24} \rho_v^{0.24}} \right) \Delta T_{sat}^{0.24} \Delta p_{sat}^{0.75} S \quad (2.13)$$

where $\Delta p_{sat}(T_w) = p_w - p_{sat}(T_{sat})$. The factor S is a suppression factor that has been introduced to account for the suppression of the nucleate boiling by the flow field. The vapor bubbles nucleating at the walls grow through a superheated liquid layer where the temperature changes. The differences are low in the case of pool boiling but during forced convection they are more significant and the bubble growth and departure from the surface are suppressed because of a thinner boundary layer and larger temperature gradients due to the increased flow velocity [2]. This has the effect that the temperatures of the bubbles T_v are lower than the wall temperature T_w and an effective superheat ΔT_e is therefore defined as

$$\Delta T_e = T_v - T_{sat} \quad (2.14)$$

The suppression factor was estimated by Chen using the ratio of the effective superheat ΔT_e and the wall superheat ΔT_{sat} as in the following expression.

$$S = \left(\frac{\Delta T_e}{\Delta T_{sat}} \right)^{0.99} \quad (2.15)$$

Chen originally correlated the suppression factor experimentally to the two-phase Reynolds number Re_{tp} and presented it graphically but it can also be expressed on functional form as [19]

$$\begin{aligned}
S &= \frac{1}{1 + 0.12Re_{tp}^{1.14}} && \text{for } Re_{tp} \leq 32.5 \\
S &= \frac{1}{1 + 0.42Re_{tp}^{0.78}} && \text{for } 32.5 < Re_{tp} < 70 \\
S &= 0.1 && \text{for } Re_{tp} \geq 70
\end{aligned} \tag{2.16}$$

The two-phase Reynolds number is the Reynolds number for the two-phase fluid where vapor bubbles are present and defined as

$$Re_{tp} = 1 \cdot 10^{-4} Re F^{1.25} \tag{2.17}$$

The factor F is a multiplier Chen introduced for saturated flow conditions to take into account larger amounts of vapor and it can be estimated through the so called Lockhart-Martinelli parameter as [29]

$$\begin{aligned}
F &= 1.0 && \text{for } X_{tt} \geq 10 \\
F &= 2.35 \left(0.213 + \frac{1}{X_{tt}} \right)^{0.736} && \text{for } X_{tt} < 10 \\
X_{tt} &= \left(\frac{1-x}{x} \right)^{0.9} \left(\frac{\rho_v}{\rho_l} \right)^{0.5} \left(\frac{\mu_l}{\mu_v} \right)^{0.1}
\end{aligned} \tag{2.18}$$

The single-phase forced convection heat transfer coefficient h_{fc} should also be multiplied with F if saturated flow conditions are present. However, for subcooled flow conditions F is set to unity as the vapor content is assumed to be very low [2].

2.6.4 The Dry-spot model

The initiation and actual mechanisms leading to the phenomenon of DNB and CHF is still not completely understood by researchers. The main reasons for this are due to that the phenomenon appears highly localized and also occur very rapidly. Furthermore, it is complicated to study the effects at the heated surfaces because of the presence of nucleate bubbles, the two-phase flow effects and the rapid movement of the interface between the phases. Because of this most information on the topic have been achieved through studies of parametric trends between system variables and CHF together with limited photographic observations. The available methods in predicting and describing the CHF phenomenon consist of "look-up tables" where data for CHF for certain geometries and conditions are tabulated together with different correlations and models mostly based on postulated mechanisms [10].

One modeling approach in predicting the DNB is that of Ha and No [3, 4, 5]. Their model is based on a concept of dry-spot formation on a heated surface. In the model, the CHF mechanism is considered to be influenced by the boiling parameters from the nucleate boiling regime and the model is therefore based on these parameters. Considering an active nucleating site where a bubble grows it is possible to define a cell area A_c around the bubble such that if a second bubble nucleate at another site in this area it will overlap with the bubble in the center. A dry-spot is considered to be formed on the surface when a certain critical number of active sites n_c are surrounding one bubble. Ha and No state that the critical number is equal to 5 [3]. The dry-spots prevent liquid to fill the liquid film microlayer that is formed under a growing bubble and the surface area will become dry. As the temperature is increased further, more dry-spots will form, accumulate and coalesce which increases the size of dry areas. As this continues the number of effective sites for bubble nucleation is significantly decreased with the effect of a reduced heat transfer and that a maximum critical heat flux is reached.

According to the model, the overall heat flux q can be expressed as the sum of the contributions q_l and q_v from the nucleate boiling and film boiling regimes respectively as

$$q = (1 - \Gamma)q_l + \Gamma q_v \tag{2.19}$$

where Γ denotes the fraction of the heated surface in contact with vapor. The model assumes a Poisson distribution of active nucleation sites and that the diameter of the cell area A_c around the active site in the

center is twice the diameter of the bubble as

$$A_c = \pi d_{av}^2 \quad (2.20)$$

where it is assumed that the bubble diameter can be represented by the time-averaged bubble diameter d_{av} . Assuming that the bubble diameter varies with time as $t^{1/2}$ the diameter can be expressed based on the bubble departure diameter d_d as

$$d_{av} = \frac{2}{3}d_d \quad (2.21)$$

Following the assumptions above the probability that a cell area A_c around an active nucleation site will include n additional active nucleation sites can be expressed as

$$P(n) = \frac{e^{-\bar{N}A_c}(\bar{N}A_c)^n}{n!} \quad (2.22)$$

The probability that the number of active nucleation sites in the cell area are greater than or equal to the critical number of active sites n_c is then expressed as

$$P(n \geq n_c) = 1 - \sum_{n=0}^{n_c-1} P(n) \quad (2.23)$$

The fraction of dry area

The fraction of dry area Γ can be estimated by assuming that the area of a dry spot A_d on the surface is equal to the base area under the bubble ($A_d = \pi d_{av}^2/4$) and that the dry spots also follow a Poisson distribution. The fraction of dry spots when all dry spots are isolated from each other Γ_i can then be expressed as the product of the area of the dry spot and the average number density of dry spots \bar{N}_d .

$$\Gamma_i = \bar{N}_d A_d \quad (2.24)$$

The average number density of dry spots can be estimated as

$$\bar{N}_d = \bar{N} P(n \geq n_c) \quad (2.25)$$

When many dry spots exist on the surface the dry spot areas will overlap with the effect of a reduction in dry area. To compensate for this Ha and No [4] discussed that the fraction of dry area is reduced by overlap from Γ_i to $x\Gamma_i$ which is equal to the actual fraction of dry area Γ . By dividing the dry spot areas into fractions f_m , where m is the number of dry spot sites within a specific dry area, they achieved an expression for x . Furthermore, by considering that the probability that any small element da of a dry spot area A_d forms part of the fraction f_m follows a Poisson distribution, the overlap variables f_m can be calculated. The argument finally result in that the actual fraction of dry area can be expressed as

$$\Gamma = 1 - e^{-\Gamma_i} \quad (2.26)$$

Active nucleation site density and bubble departure diameter

The average number density of active nucleation sites \bar{N} and bubble departure diameter d_d are two important parameters to express. The average active nucleation site density can be estimated from the following correlation [30].

$$\bar{N}' = f(\rho') R'_c \quad (2.27)$$

Here \bar{N}' is the dimensionless nucleation site density and $f(\rho')$ and R'_c is a pressure dependent function and the dimensionless cavity radius respectively expressed as

$$\begin{aligned} R'_c &= 2R_c/d_d \\ f(\rho') &= 2.157 \cdot 10^{-7} \rho'^{-3.2} (1 + 0.0049\rho')^{4.13} \\ \rho' &= (\rho_l - \rho_v)/\rho_v \end{aligned} \quad (2.28)$$

where R_c is the critical cavity size. By estimating these parameters it is possible to compute the average nucleation site density as

$$\bar{N} = \frac{\bar{N}'}{d_d^2} \quad (2.29)$$

The critical cavity size can be estimated from the following expression.

$$R_c = \frac{2\sigma(1 + (\rho_v/\rho_l))/p_l}{\exp(i_{lv}(T_v - T_{sat})/(R_v T_v T_{sat})) - 1} \quad (2.30)$$

The bubble departure diameter is the diameter of the vapor bubble when it lifts off from the heated surface and it can be estimated from the Fritz equation. The Fritz equation for bubble departure diameter was derived from a balance between buoyancy and surface tension forces and is expressed as

$$d_{dF} = 0.0208\theta \left(\frac{\sigma}{g(\rho_l - \rho_v)} \right)^{1/2} \quad (2.31)$$

where θ is the bubble contact angle given in degrees and defined as previously described in figure 2.4. The vapor temperature T_v in equation 2.30 is the temperature of the vapor in the nucleating bubbles that grows through the superheated liquid layer at the wall. Because the temperature changes drastically across the superheated layer the temperature of the bubbles will be somewhat lower than that of the wall. One way to estimate the temperature T_v is to use the concept of a suppression factor S and an effective superheat ΔT_e as introduced in the Chen correlation in section 2.6.3. The effective superheat is defined as

$$\Delta T_e = T_v - T_{sat} \quad (2.32)$$

and since the suppression factor was defined by Chen as

$$S = \left(\frac{\Delta T_e}{\Delta T_{sat}} \right)^{0.99} \quad (2.33)$$

the effective superheat can be expressed as follows by simplifying the expression with power 1.0 instead of 0.99.

$$\Delta T_e = S\Delta T_{sat} \quad (2.34)$$

2.6.5 Film boiling

The heat transfer during film boiling can be estimated from the following expression from the study of film boiling on a vertical surface by Bui and Dhir [31]. This is the expression that was used by Ha and No [4].

$$q_v = 0.37 \left[\frac{k_v^3 \rho_v (\rho_l - \rho_v) g i_{lv}}{\mu_v \sqrt{\sigma/g(\rho_l - \rho_v)}} \right]^{1/4} \Delta T_{sat}^{3/4} \quad (2.35)$$

3 Method

A method to predict and describe the heat transfer in subcooled flow boiling has been developed and evaluated using a Matlab code. The final method is implemented in the commercial CFD software Star-CCM+ and applied to a simplified test case geometry. To investigate how the method perform for more realistic conditions it is also applied to an engine cooling jacket under operational conditions. The implementation and simulation setup in Matlab and Star-CCM+ are here described together with a presentation of fluid properties and the assumptions and limitations of the used models and correlations. All results are presented in chapter 4.

3.1 Properties of vapor and coolant mixture

In most engine cooling systems a coolant mixture is used instead of a pure liquid like water. This is mainly due to better antifreeze protection, an increased boiling point and improved resistance to corrosion. The coolant liquid that has been considered throughout this work is a 50-50 percent mixture of water and the antifreeze liquid BASF Glythermin NF. Glythermin NF is based on ethylene-glycol with some smaller additions of substances to for example increase resistance to corrosion. The properties of the mixture differ from that of pure water. For example, the boiling point at a pressure of 2 bar is 120.4 °C for pure water and 130.7 °C for the coolant mixture. The boiling point for the pure antifreeze liquid is even higher, around 225.4 °C [32, 33]. At the boiling point of the mixture the generated vapor will consist of only water. Therefore, values for water vapor have been assumed for the properties of vapor during the work and are taken from the Knovel engineering database [34] and the open steam table database XSteam [35]. The liquid properties of the coolant mixture are taken from the BASF Glythermin technical information sheet [33]. Expressions for the properties variation with temperature are curve fitted for the pressure of 2 bar. Furthermore, it is assumed that the vapor generation does not effect the composition of the mixture.

3.2 Modeling setup

The temperature of the bulk flow in the cooling system of an engine is normally controlled to be below the boiling point and differs only a few degrees between inlet and outlet. However, boiling can still occur locally in the system and is in this work assumed to be subcooled flow boiling. This means that the temperature of the bulk liquid is lower than the saturation temperature of the liquid and that the vapor bubbles that depart from the hot surfaces almost immediately condensate and mix with the bulk flow. This can motivate the use of a single-phase flow model during simulations, which has been used during this study. When a more significant amount of vapor is assumed to be present in the system, a multiphase framework can be more favourable to use to better describe the effects of a second phase.

Convective heat transfer

Before boiling is present the heat transfer is assumed to consist of convection and is described in the simulations in Matlab by the Dittus-Boelter correlation (equation 2.4). Although the Dittus-Boelter correlation is widely used it is a simple expression correlated for very specific conditions. For example, the assumptions of smooth surfaces and fully developed flow is often not the case in reality, especially for the conditions in an engine cooling jacket. To improve the predictions of the correlation, it is possible to extend it with certain factors to take into account a variety of aspects such as differences in surface roughness, coolants, velocities and temperatures [8]. In this work the standard Dittus-Boelter correlation is used without any further additions when evaluating the modeling methods in Matlab. For the implementation in Star-CCM+ both the already built-in method for convection and the Dittus-Boelter correlation are used and compared.

Nucleate boiling heat transfer

To predict when boiling starts the ONB criteria of Hsu is used (equation 2.11). After this point the heat transfer is described by a nucleate boiling part and a convective part according to the Chen correlation (eq. 2.12). The convective part is computed in the same way as for the single-phase convection before boiling, with the Dittus-Boelter correlation in Matlab and using either the built-in model or the Dittus-Boelter correlation in Star-CCM+. The reader should be aware of that the Chen correlation was originally correlated for vertical

channel flows with axisymmetric heating for pure liquids. It might not therefore give the same accuracy for a more complex system such as an engine cooling jacket. The Chen correlation is here used as a first step in developing a method to model subcooled boiling in engine cooling systems. This mainly because of its previous use to similar applications within the field, where the heat transfer trends were captured with success, and no other correlation gave continuously better results for the applications in the studies (section 2.5).

Regarding the use of saturation temperature within the correlations and models, the ONB temperature is first computed using the parameters of the liquid at saturation temperature. After this, the ONB temperature is used instead of the saturation temperature when the correlations and models are computed. Furthermore, the Chen correlation is computed using volume averaged bulk properties of the flow.

Departure from Nucleate Boiling (DNB) and Critical Heat Flux (CHF)

The Chen correlation is only valid in the nucleate boiling regime and as a means to set an upper limit for when the correlation is applied, the so called Dry-spot model is used to indicate and describe when the DNB starts and the transition region follows. It should be noted that the DNB and CHF are still not completely understood by researchers and it is hard to estimate it with good accuracy for complex systems. Here the Dry-spot model is therefore only used to set an upper limit for the heat transfer and thereby give more robustness to the simulations and wider applicability. Together with the Dry-spot model, the film boiling correlation of Bui and Dhir (equation 2.35) is used in this work similarly as by Ha and No [4]. No further investigation on film boiling correlations has been performed since it is not within the scope of this thesis.

An uncertain parameter with large impact on the DNB predictions of the Dry-spot model is the bubble contact angle θ . The effect of this parameter on the boiling curve is investigated during the simulations in Matlab. For the other simulations a value of 30° is chosen to be able to observe the trends. The impact of various other conditions such as orientation, surface roughness and vibrations have not been studied in this work, apart from what is included in the used models. For example regarding surface roughness, a wide range of active nucleating cavities is assumed when predicting the ONB from the condition of Hsu (equation 2.11) but smooth surfaces are considered when modeling the flow field.

3.3 Simulations in Matlab

As a first step a Matlab code has been created where the correlations and models are implemented to be able to simplify the evaluation. A purpose of the Matlab code is to examine if and how the implementation of the models can be performed. The code is also used to get an understanding of the models, how the heat transfer is described and if the results are as expected. In Matlab a cross-section of a duct flow has been studied with constant bulk flow properties. The heat transfer occur from the heated walls to the bulk flow and is studied in one dimension. A temperature boundary condition is set for the walls and the temperature is increased continuously to investigate the behaviour of the boiling curve. The simulations are performed with the following set-up

- ONB condition + Chen correlation
- ONB condition + Chen correlation + Dry-spot model

where also the film boiling correlation of Bui and Dhir are part of the Dry-spot model. Apart from the trends and behaviour of the models, the following parameters are studied in detail to see what impact they have on the predictions of the heat transfer.

- Inlet velocity V
- Subcooling ΔT_{sub}
- Suppression factor S
- Bubble contact angle θ

The simulation setup and the range of conditions that are used and studied in Matlab are presented in table 3.1.

Table 3.1: Values and conditions used during simulations in Matlab

Parameter	Value
Duct width, a [m]	0.016
Duct height, b [m]	0.01
Hydraulic diameter, d_h [m]	0.0123
System pressure, p [bar]	2
Wall temperature, T_w [°C]	90 – 250
Subcooling, ΔT_{sub} [°C]	0, 10, 20, 40
Inlet velocity, V [m/s]	0.25, 1, 3, 5
Suppression factor, S	0.1 – 1.0
Bubble contact angle, θ [°]	10, 30, 60, 90

3.4 Simulations in Star-CCM+

Simulations in Star-CCM+ have been performed in two parts. The first part is simulations of a simple test case, where the implemented models are analysed and evaluated further. The models are then applied to the case of an engine cooling jacket at operational conditions to study how the models perform for a real case application. Both the test case and the engine cooling jacket are simulated using conjugate heat transfer models, where both solid structure and fluid volume are included in the simulations. Only thermal effects are considered for the solid part. The test case is also run without conjugate heat transfer to compute boiling curves with only the fluid volume included in the simulations.

3.4.1 Implementation of models

The models are implemented in Star-CCM+ as a set of user defined field functions in combination with the function User Defined Wall Heat Flux Specification. The field functions can be coupled by using field functions within each other and conditional operators such as an if statement can also be defined in a field function. The User Defined Wall Heat Flux Specification is activated on surfaces or interfaces of the model and makes it possible to add an addition to the heat flux. The addition to the heat flux is defined by specifying four coefficients originating from the following linearized expression for the wall heat flux q_w

$$q_w = A + BT_c + CT_w + DT_w^4 \quad (3.1)$$

where T_c is the temperature in the cell closest to the wall and T_w is the wall temperature. The coefficients A - D are divided into an internally computed part and a user defined part as

$$\begin{aligned} A &= A_{internal} + A_{user} \\ B &= B_{internal} + B_{user} \\ C &= C_{internal} + C_{user} \\ D &= D_{internal} + D_{user} \end{aligned} \quad (3.2)$$

The internal coefficients are computed by the built-in methods for heat transfer in Star-CCM+, for example convection or radiation. The user defined coefficients are the ones that can be specified by the user to add an addition to the wall heat flux. Numerically, the internal coefficients are computed first and then the user defined coefficients are added to arrive at the net wall heat flux coefficients. It is not possible to change the internal coefficients directly but expressions representing the internal coefficients can be used and included in the user defined coefficients. This makes it possible to completely remove the internal coefficient $A_{internal}$ and define the net coefficient A as a function F by specifying the user defined coefficient A_{user} as

$$A_{user} = F - A_{internal} \quad (3.3)$$

which give the net coefficient as

$$A = A_{internal} + (F - A_{internal}) = F \quad (3.4)$$

In this work the user defined coefficient A_{user} has primarily been used when implementing the boiling heat transfer models and correlations [25].

The Chen correlation

The Chen correlation is implemented by defining field functions in accordance with the expressions introduced in section 2.6.3 to get the nucleate boiling part of the wall heat flux q_{nb} . The field function for q_{nb} is implemented as a conditional expression where the heat flux takes a value only if the ONB condition is satisfied, otherwise the function is zero. The coefficients in the User Defined Wall Heat Flux Specification are then defined as

$$\begin{aligned} A_{user} &= -q_{nb} \\ B_{user} &= 0 \\ C_{user} &= 0 \\ D_{user} &= 0 \end{aligned} \tag{3.5}$$

Here the negative sign before q_{nb} is needed because the heat flux is defined as positive out from the fluid domain. When the net coefficients are assembled, the addition from the built-in convective heat transfer in Star-CCM+ is also included from the internal coefficients. If the built-in methods for convective heat transfer are replaced with the convective heat transfer correlation by Dittus-Boelter, the user defined coefficients should instead be given as

$$\begin{aligned} A_{user} &= -A_{internal} - (q_{nb} + q_{fc}) \\ B_{user} &= -B_{internal} \\ C_{user} &= -C_{internal} \\ D_{user} &= -D_{internal} \end{aligned} \tag{3.6}$$

where q_{fc} is the convective heat flux computed according to the Dittus-Boelter correlation in section 2.6.1.

The Chen correlation and the Dry-spot model

To also include the Dry-spot model in the simulations, the different parts of the Dry-spot model in section 2.6.4 are implemented using field functions together with the correlation for film boiling in section 2.6.5. The transition to film boiling at the DNB is governed by the fraction of dry area Γ . For the heat flux during film boiling q_v , no convection should be present. The coefficients when using the Chen correlation in combination with the Dry-spot model are then expressed as

$$\begin{aligned} A_{user} &= -A_{internal} + (1 - \Gamma)(-q_{nb} + A_{internal}) - \Gamma q_v \\ B_{user} &= -B_{internal} + (1 - \Gamma)B_{internal} \\ C_{user} &= -C_{internal} + (1 - \Gamma)C_{internal} \\ D_{user} &= -D_{internal} + (1 - \Gamma)D_{internal} \end{aligned} \tag{3.7}$$

when the built-in method for convection in Star-CCM+ is used in the Chen correlation. When the Dittus-Boelter correlation is used instead of the built-in method, the expressions are modified in accordance with equation 3.6.

Limitation of the nucleate boiling heat flux

When specifying an addition to the wall heat flux with the Chen correlation using the User Defined Wall Heat Flux Specification, the addition is forced at the wall. And since the nucleate boiling part in the Chen correlation is not directly dependent on the cell temperature of the fluid adjacent to the wall, unrealistically high heat fluxes can occur for higher wall temperatures. This can especially be the case when the correlation is applied outside its range of applicability, for example when film boiling is present. The consequence is non-physical fluid temperatures where the cell temperature can become higher than the temperature of the wall. As an approximation to account for this when non-conjugate heat transfer simulations are performed, the maximum temperature of the fluid is limited to the wall temperature. This is not as straightforward to do when performing conjugate heat transfer simulations, since a constant wall temperature is not set. A factor SF is instead implemented and multiplied with the heat flux of the Chen correlation. The factor takes the value of 1 if the cell temperature adjacent to the wall is lower than the wall temperature and a value of 0 if the cell temperature becomes higher than the wall temperature.

An alternative to increase robustness of the simulations is to decrease the addition of the nucleate boiling part slowly when the cell temperature is larger than the wall temperature. This is performed by defining the SF factor as

$$SF = \max \left[0, \min \left(\left(\frac{T_w - T_c}{T_w - T_{sat}} \right), 1 \right) \right] \quad (3.8)$$

where T_c denotes the temperature of the cell adjacent to the wall. When $T_c > T_w$ the nucleate boiling heat flux is zero and if $T_c = T_{sat}$ the correlation is used directly. For temperatures in between, a fraction of the overall heat flux from the nucleate boiling part is used. In this case the saturation temperature T_{sat} is used as a reference but another temperature can be used such as a certain temperature below the wall temperature.

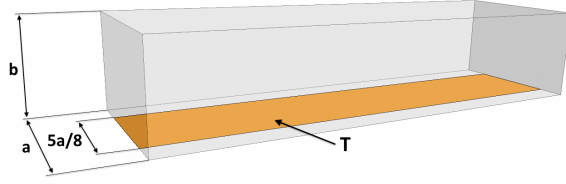
Scalar indicators

As a tool to predict the ONB and DNB two scalar indicators have been implemented into Star-CCM+ to visually observe where boiling is predicted. From the ONB condition (equation 2.11) a scalar field function is defined taking the value of 1 if boiling is predicted, i.e. if $\Delta T_{sat} > \Delta T_{sat,ONB}$, and 0 otherwise. The field function is called ONB scalar indicator. Because the ONB condition is computed using the single-phase convective heat transfer coefficient, the scalar indicator can be used independently of the boiling heat transfer correlations.

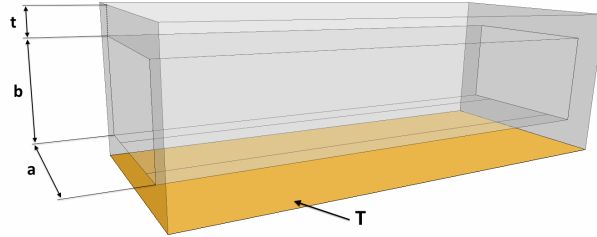
The second scalar indicator is an extension to the first with the addition of also indicating if DNB has been initiated. The function is called boiling scalar indicator and the DNB is defined to start if the parameter Γ from the Dry-spot model (equation 2.19) is larger than 0.001. The boiling scalar indicator takes the value of 1 if ONB is achieved, 2 if DNB has been initiated and 0 when no boiling is present. For this scalar indicator, the nucleate boiling heat transfer correlation of Chen needs to be included in the simulations. The Dry-spot model is also needed to be solved, but it is possible to run it on the side and not activated when computing the boiling heat transfer.

3.4.2 Test case

The geometry of the test case has been created similarly as the test case used in the PhD thesis by Robinson [8]. The shape and dimensions of the geometry are aimed at representing the complex geometry of an engine cooling jacket in a more simple form and consist of a 50 mm long rectangular duct with width $a = 16$ mm and height $b = 10$ mm. To evaluate the boiling curve, non-conjugate heat transfer simulations are performed on the fluid volume of the test case as presented in figure 3.1a. The simulations are performed at different settings with a constant temperature boundary condition set for the heater plate. The temperature of the heater plate is varied between 90-225 °C, with a step of 1 °C, to achieve boiling curves for the wall heat flux versus wall temperature. The boiling models are also applied to conjugate heat transfer simulations on the test case geometry presented in figure 3.1b to evaluate how they perform for this type of simulations. During these simulations a constant temperature is set at the outer bottom wall of the solid. The thickness t of the solid walls is 3 mm. For both simulation cases a 75 mm inlet region and a 125 mm outlet region are added to the test section to prevent boundary effects and to achieve a more developed flow profile. The boiling heat transfer models are activated on the heater plate for the non-conjugate heat transfer simulations and on all solid-fluid interfaces during the conjugate heat transfer simulations. The complete boundary conditions that are set for each simulation case are presented in table 3.2. The bulk properties used in the Chen correlation and for calculation of the suppression factor are taken as volume averages over the test case domain. For the solid part during the conjugate heat transfer simulations the built-in material properties for aluminium alloy are used.



(a) The geometry used for non-conjugate heat transfer simulations with the heater plate colored.



(b) The geometry used for conjugate heat transfer simulations. The temperature boundary condition is here set at the bottom outer wall.

Figure 3.1: The two geometries of the test case.

Table 3.2: Boundary conditions for the simulations of the test case.

Non-conjugate heat transfer	
Inlet	Velocity inlet, $T = 90\text{ }^\circ\text{C}$
Outlet	Pressure outlet, $p = 2\text{ bar}$
Heater plate	Wall, Constant temperature T_w , Heat transfer models
All other surfaces	Wall, Adiabatic
Conjugate heat transfer	
Inlet	Velocity inlet, $T = 90\text{ }^\circ\text{C}$
Outlet	Pressure outlet, $p = 2\text{ bar}$
Solid-Fluid interfaces	Wall, Heat transfer models
Outer bottom solid surface	Wall, Constant temperature T_w
All other surfaces	Wall, Adiabatic

The CFD solver set-up and mesh settings that are used for the simulations are presented in table 3.3 and an overview of the different simulations that are performed can be studied in table 3.4. Case 1-4 are run with the aim to compute boiling curves. This is performed using the combination of the Chen correlation and the Dry-spot model, but also using only the Chen correlation to evaluate the impact from the Dry-spot model. Because it is hard to determine if the implemented boiling models affect the already built-in heat transfer method for convection in Star-CCM+, case 5 and 6 are performed with the Dittus-Boelter correlation replacing the built-in method for convection. Using the Dittus-Boelter correlation is a more straightforward method since it is easier to control by the user. Case 5 and 6 are performed with boiling models applied in the same way as for case 1-4 to be able to study the differences in boiling curves. All simulations for case 1-6 are performed with the the maximum allowable temperature of the fluid limited to the temperature of the wall. To investigate the effects of not limiting the temperature, case 7 and 8 are performed using only the Chen correlation applied and no limitation of the temperature.

The simulations of the conjugate heat transfer case 9-13 are performed with a constant temperature applied to the outer bottom solid wall. The simulations are run with only convective heat transfer with the aim to present the predictions of the ONB scalar indicator for different flow velocities. Case 14-16 are essentially the same case, but with different heat transfer models activated to be able to compare the differences in temperature. Case 14 is run with only convective heat transfer and case 15 and 16 are run with the Chen correlation and the combination of the Chen correlation and the Dry-spot model, respectively. The boiling scalar indicator is evaluated for case 15, where the Dry-spot model is computed but not active in the boiling heat transfer calculation.

Table 3.3: *CFD solver and mesh settings for the test case.*

Solver settings	
Steady RANS	
Segregated flow solver	
Segregated fluid temperature solver	
SST $k-\omega$ turbulence model	
Mesh settings	
Mesh type:	Polyhedral
Number of inflation layers:	14
Number of cells:	~ 2 million
Base size:	0.5 mm
Wall y^+ :	< 1

Table 3.4: *An overview of the simulations of the test case geometry.*

Non-conjugate heat transfer				
Case	Inlet velocity [m/s]	Convection model	Max temperature	
1	0.25	Star-CCM+	T_w	
2	1.00	Star-CCM+	T_w	
3	3.00	Star-CCM+	T_w	
4	5.00	Star-CCM+	T_w	
5	0.25	Dittus-Boelter	T_w	
6	3.00	Dittus-Boelter	T_w	
7	0.25	Star-CCM+	N/A	
8	3.00	Star-CCM+	N/A	
Conjugate heat transfer				
Case	Inlet velocity [m/s]	Solid temperature [$^{\circ}$ C]	Convection model	Boiling model
9	3.00	170	Star-CCM+	-
10	4.00	170	Star-CCM+	-
11	4.50	170	Star-CCM+	-
12	4.75	170	Star-CCM+	-
13	5.00	170	Star-CCM+	-
14	3.00	225	Star-CCM+	-
15	3.00	225	Star-CCM+	Chen
16	3.00	225	Star-CCM+	Chen + Dry-spot

3.4.3 Engine cooling jacket

Apart from the simulations of the test case, the boiling models and scalar indicators have also been applied to a conjugate heat transfer case of a 4-cylinder petrol engine cooling jacket at operating conditions. The geometry of the fluid domain of the cooling jacket that is considered in this work is presented in figure 3.2. The cooling jacket consists of one part in the cylinder block and one part in the cylinder head. The inlet is located at the second cylinder on the block part and there are two outlets: one located on the other side of cylinder two in the block part going to the thermostat and one at the top of the first cylinder in the head part going to the cabin heater. Since conjugate heat transfer simulations are performed, the solid structure surrounding the fluid domain is also included in the simulations.

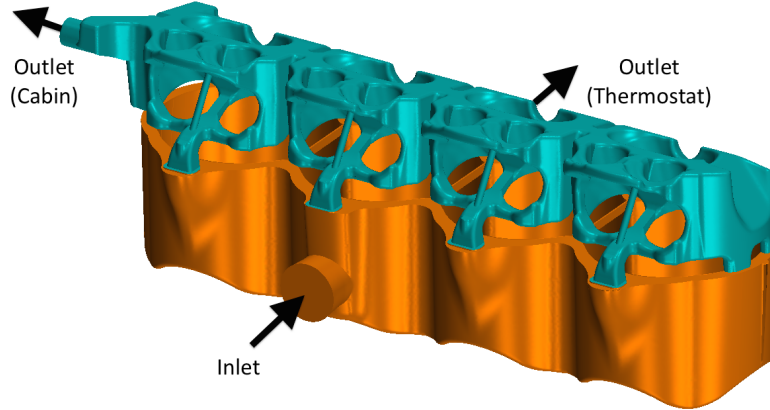


Figure 3.2: The geometry of the fluid domain of the engine cooling jacket. It is divided into two parts: one in the cylinder head (the upper part) and one in the cylinder block (the lower part).

Compared to the rectangular duct geometry of the test case, it is not that straightforward to define the bulk properties for the much more complex geometry of the cooling jacket. As an approximation, the bulk flow properties are taken as volume averages of the fluid domain. Another issue is to define a representative hydraulic diameter for the cooling jacket. Based on measurements in the geometry, a hydraulic diameter of 0.01 m is used in the simulations as an estimation.

The original set-up for the conjugate heat transfer case of the cooling jacket has been provided by Volvo Cars. Three different simulations are prepared to be able to compare the predictions of the models. One simulation with the built-in method for convection, one with the Chen correlation applied and finally one where also the Dry-spot model is used. The boundary conditions for the fluid part of the conjugate heat transfer case is presented in table 3.5. The heat input from combustion is specified by heat transfer coefficients in the solid domain. A description of the mesh and solver settings are presented in table 3.6.

Table 3.5: Boundary conditions for the fluid domain of the conjugate heat transfer simulations of the engine cooling jacket.

Boundary conditions	
Inlet	Pressure inlet, $p = 2$ bar Temperature, $T_{\text{inlet}} = 90$ °C
Outlet 1 Cabin	Mass flow outlet, $\dot{m} = 0.3$ kg/s
Outlet 2 Thermostat	Mass flow outlet, $\dot{m} = 1.7$ kg/s
Solid-fluid interfaces	Wall, Heat transfer models

Table 3.6: *CFD solver and mesh settings for the conjugate heat transfer simulations of the engine cooling jacket.*

Solver settings	
Steady RANS	
Segregated flow solver	
Segregated fluid temperature solver	
k- ϵ realizable turbulence model	
Two-layer All y^+ Wall treatment	
Mesh settings	
Mesh type:	Polyhedral
Number of cells:	~ 11.2 million
Base size:	2.0 mm

4 Results

4.1 Simulations in Matlab

The simulations in Matlab have been performed according to section 3.3. The results are mainly presented in the form of boiling curves, where the wall heat flux q_w is plotted against the wall temperature T_w . The impact on the heat transfer when taking nucleate boiling into account can clearly be seen in figure 4.1, where the Chen correlation is compared to using only a convective model for the velocity of 1 m/s. The convective part is here described by the Dittus-Boelter correlation (section 2.6.1) and the initiation of nucleate boiling is predicted by the ONB condition of Hsu (equation 2.11). After the ONB, there is a significant increase in wall heat flux for an increase in wall temperature if the Chen correlation is applied. If only convective heat transfer is accounted for, a much lower heat flux is predicted and the estimation of the cooling effects in the nucleate boiling regime is inaccurate.

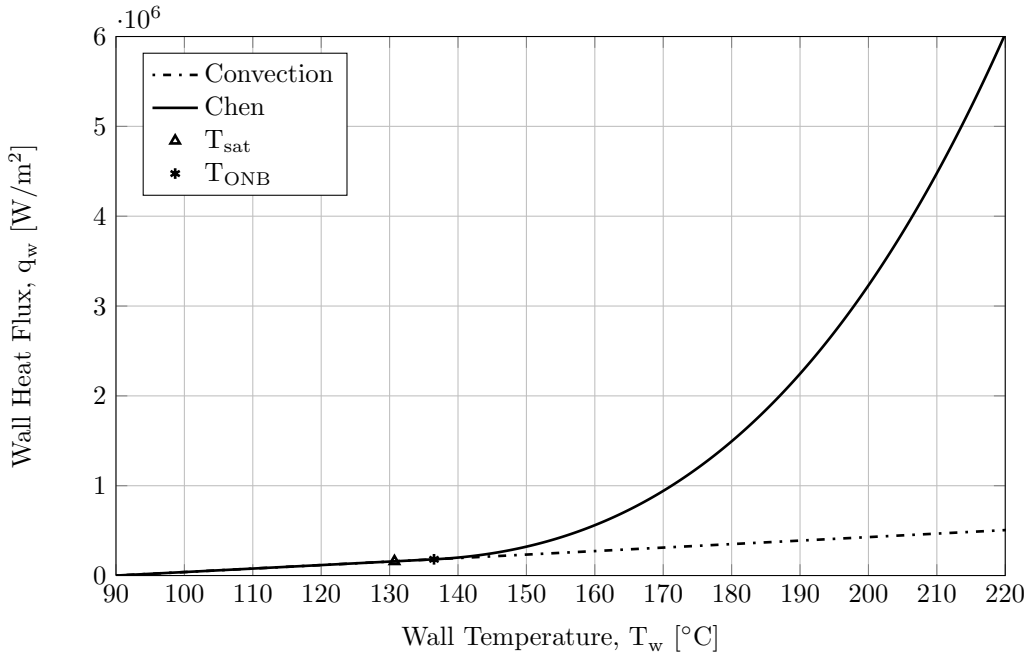


Figure 4.1: Wall heat flux predictions with the Chen correlation for inlet velocity $V = 1$ m/s and inlet subcooling $\Delta T_{sub} = 40$ °C.

The predictions of the Chen correlation are not valid if the correlation is applied outside the nucleate boiling regime. To estimate and set an upper limit for the Chen correlation, the Dry-spot model has been used to describe the transition from nucleate boiling to film boiling. The results when including the Dry-spot model can be seen in figure 4.2. Note the different scales in the figures. When adding the Dry-spot model the point of DNB is predicted. After this point, the contribution to the heat flux from the Chen and Dittus-Boelter correlations decreases and is gradually replaced by the film boiling heat transfer correlation of Bui and Dhir. The transition results in a very rapid decrease in heat transfer.

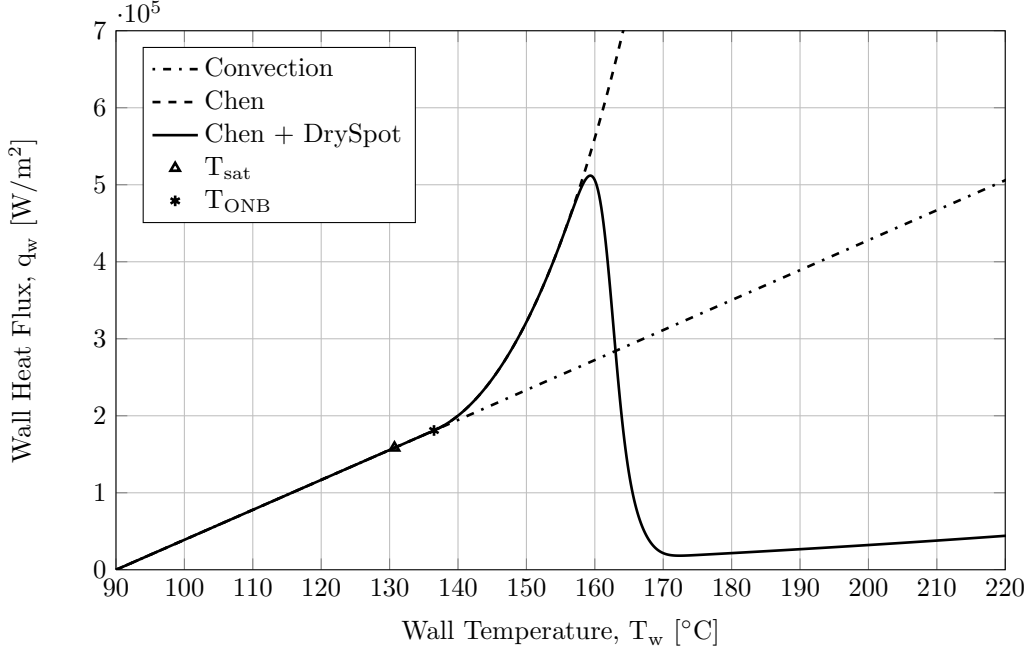


Figure 4.2: Wall heat flux predictions with the Dry-spot model for inlet velocity $V = 1$ m/s, inlet subcooling $\Delta T_{sub} = 40$ °C and bubble contact angle $\theta = 30$ °.

4.1.1 Effects of velocity

To study the effects of velocity on the ONB and heat transfer predictions, the boiling models have been run for the four velocities 0.25, 1, 3 and 5 m/s. The resulting predictions of the ONB temperature and the Chen suppression factor S can be seen in table 4.1. An increase in velocity has the effect of an increase in ONB temperature. This means that the boiling will start at a lower temperature for lower velocities and the initiation of boiling will approach the saturation temperature. The decrease of the suppression factor with an increase in velocity indicates that the nucleate boiling is suppressed for higher velocities. The impact of velocity on the predictions of the Chen correlation is also presented graphically in figure 4.3. The effects of increased velocity on the convective heat transfer is evident in the beginning of the curves, where the heat fluxes are higher for an increase in velocity. As the wall temperature increases, the curves start to coincide whereupon the heat fluxes for lower velocities become higher than the heat fluxes for higher velocities. The heat transfer predictions when the Dry-spot model is included are presented in figure 4.4. The bubble contact angle is here set to 30 °. It can here be seen that for this value, the DNB and the transition region start before the curves coincide. It can also be noted that the DNB occurs later for a higher velocity.

Table 4.1: The effect of velocity on the ONB temperature and the suppression factor S in the Chen correlation. The saturation temperature of the mixture is 130.7 °C.

Velocity [m/s]	T_{ONB} [°C]	S
0.25	133.9	0.9628
1.00	136.5	0.8419
3.00	140.0	0.6034
5.00	142.3	0.4594

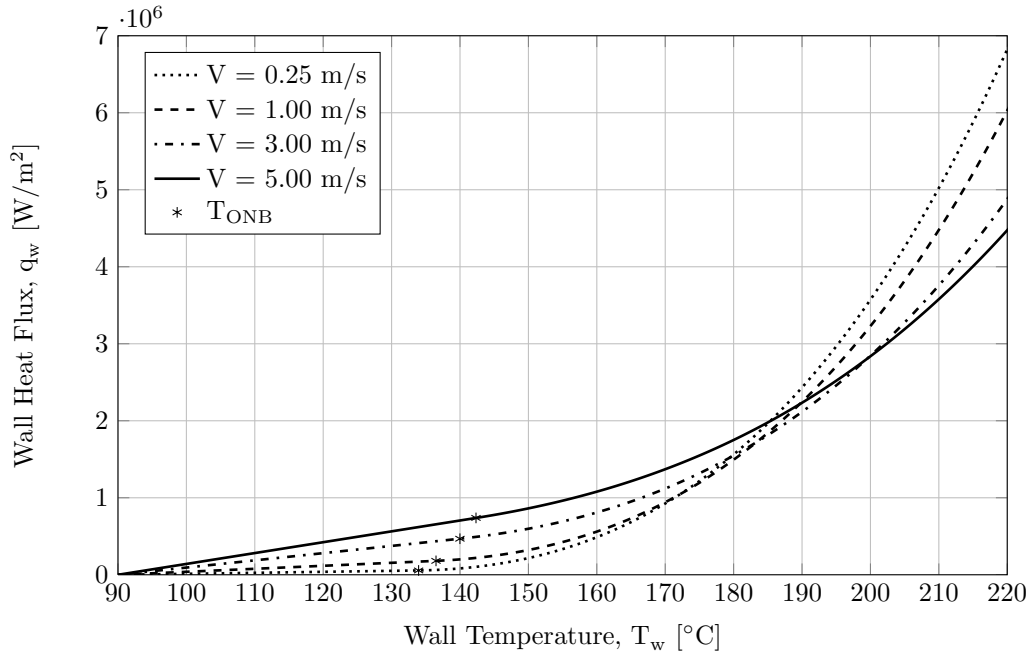


Figure 4.3: Wall heat flux predictions using the Chen correlation for different velocities at inlet subcooling $\Delta T_{sub} = 40^\circ\text{C}$.

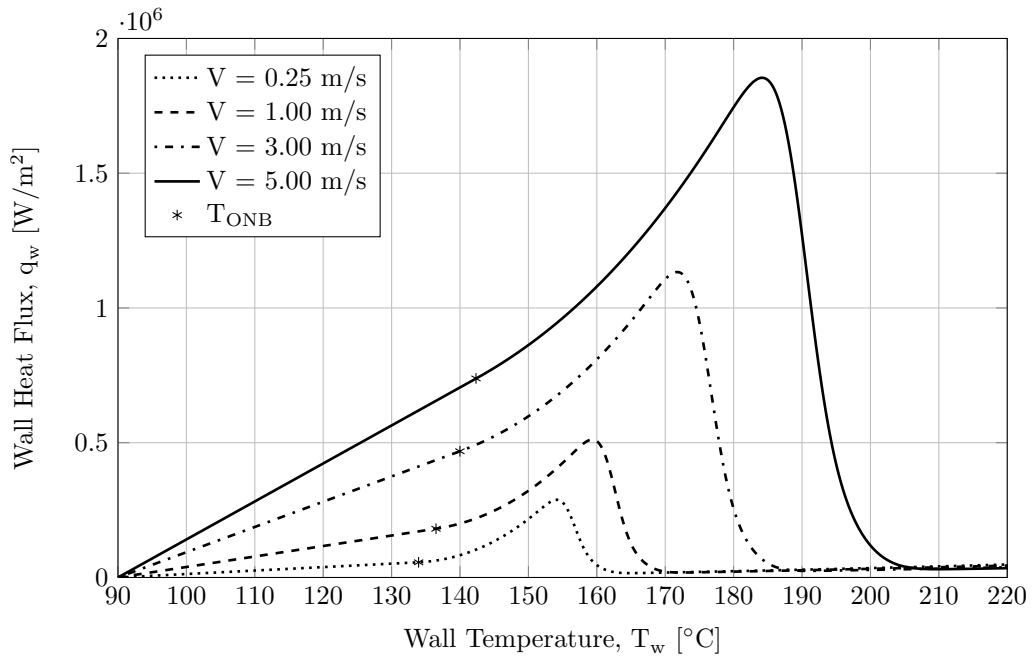


Figure 4.4: Wall heat flux predictions using the Chen correlation and the Dry-spot model for different velocities for inlet subcooling $\Delta T_{sub} = 40^\circ\text{C}$ and bubble contact angle $\theta = 30^\circ$.

4.1.2 Effects of suppression factor

The suppression factor S , as defined in the Chen correlation, is a factor with the purpose to account for the suppression of nucleate boiling due to the forced convection. The factor is defined in equation 2.16 in section 2.6.3 as dependent on the Reynolds number, which means that it is affected by the velocity of the flow field as can be seen in table 4.1. Since the suppression factor is multiplied with the addition to the heat transfer due to nucleate boiling in the Chen correlation, the heat transfer mechanism will approach pure convective heat transfer when the factor approaches zero, i.e. with increased velocity. This behaviour is illustrated in figure 4.5, where the value of the suppression factor is set explicitly between 0 and 1 for simulations with inlet velocity of $V = 1$ m/s and subcooling $\Delta T_{sub} = 40$ °C. Apart from the direct scaling effect of the nucleate boiling part in the Chen correlation, the suppression factor is also used in the Dry-spot model to estimate the temperature of the growing vapor bubbles through the effective superheat ΔT_e . From the definition in equation 2.34 in section 2.6.4, the effective superheat approaches the wall superheat ΔT_{sat} for pool boiling conditions as the suppression factor approaches 1. This means that the temperature of the growing vapor bubbles approach the wall temperature for an increased suppression factor. It can be noted that for higher values of the suppression factor, the DNB is initiated earlier. This can be seen in figure 4.6 where results are presented for simulations where also the Dry-spot model is included.

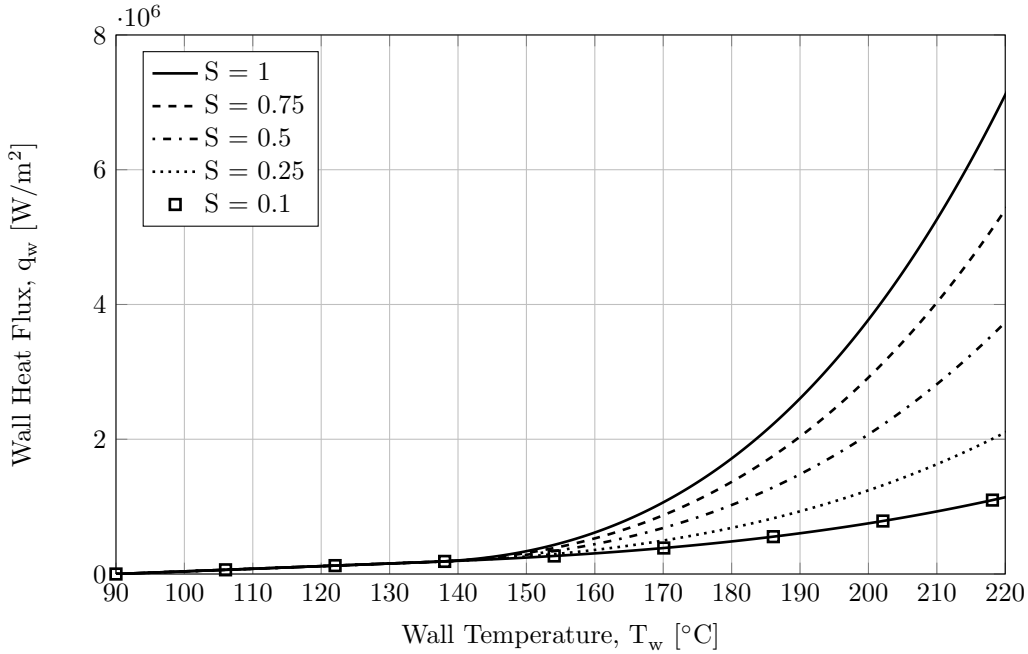


Figure 4.5: The predictions of the Chen correlation for different constant values of the suppression factor S for an inlet velocity of $V = 1$ m/s and subcooling $\Delta T_{sub} = 40$ °C.

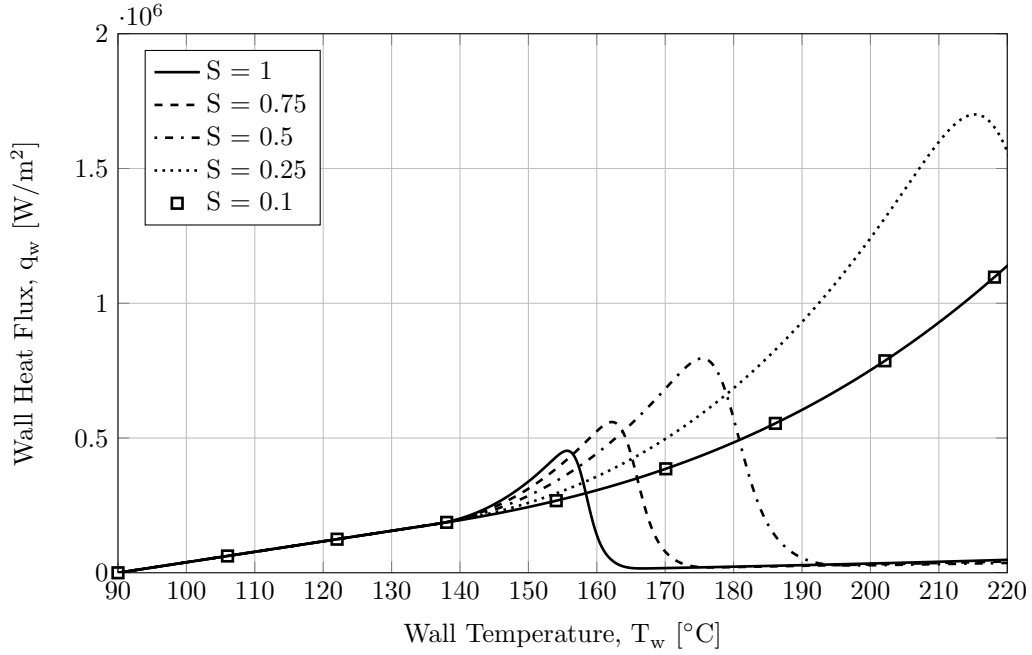


Figure 4.6: The predictions of the Chen correlation together with the Dry-spot model for different constant values of the suppression factor S for an inlet velocity of $V = 1$ m/s, subcooling $\Delta T_{sub} = 40^\circ\text{C}$ and bubble contact angle $\theta = 30^\circ$.

4.1.3 Effects of inlet subcooling

The inlet subcooling ΔT_{sub} is part of the convective heat transfer correlation and the ONB condition by Hsu. To investigate the effects of varying inlet subcooling on the predictions of the heat transfer, simulations have been run for four different degrees of subcooling. The results can be seen in figure 4.7 for the Chen correlation and in figure 4.8 where also the Dry-spot model is applied. Note the difference in scales of the two figures. The effects are, as expected, mainly seen for the convective heat transfer and the ONB temperature. An increase in subcooling increases the convective part of the heat transfer slightly as well as the temperature of ONB. There are no significant effects on the heat transfer at higher wall temperatures when the Dry-spot model is applied.

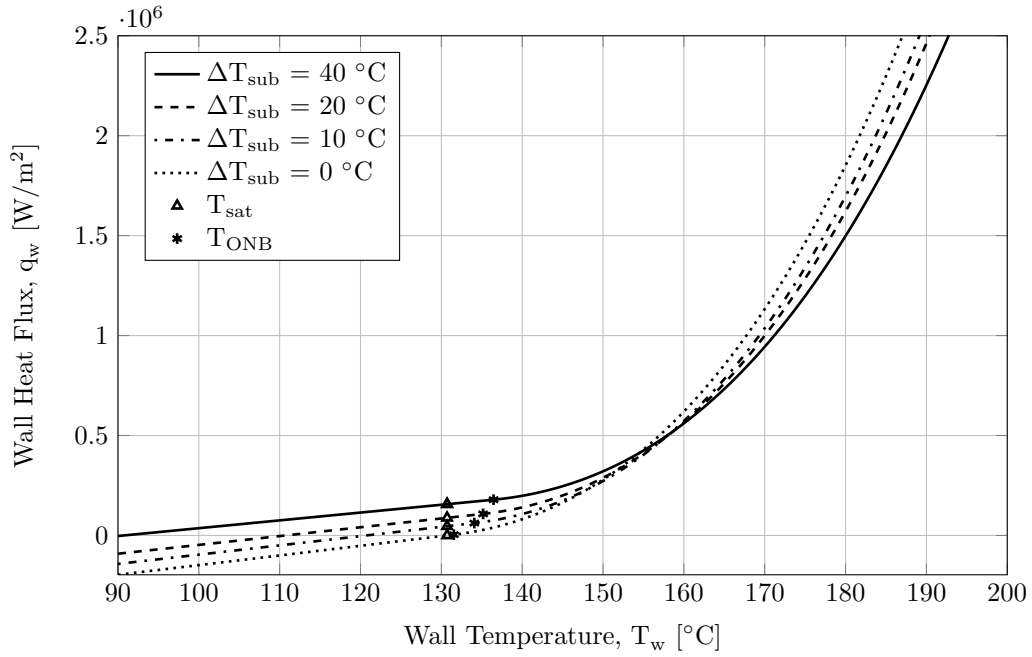


Figure 4.7: The heat transfer predictions of the Chen correlation for different degrees of subcooling ΔT_{sub} for an inlet velocity of $V = 1$ m/s.

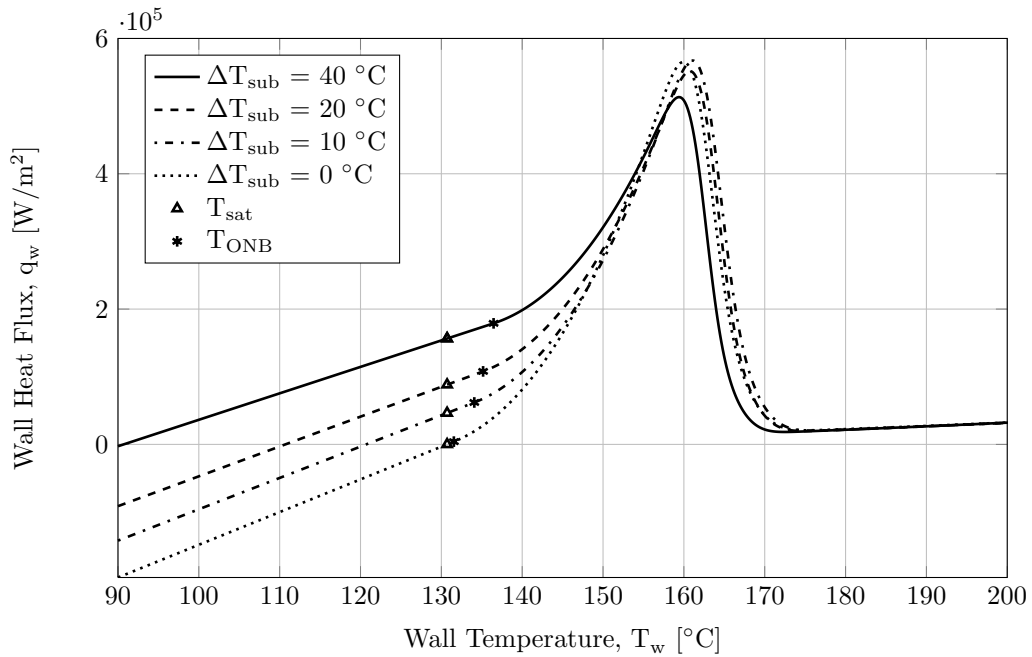


Figure 4.8: The heat transfer predictions of the Chen correlation together with the Dry-spot model for different degrees of subcooling ΔT_{sub} for an inlet velocity of $V = 1$ m/s and bubble contact angle $\theta = 30^\circ$.

4.1.4 Trends of bubble departure diameter and active nucleation site density

The bubble departure diameter and the active nucleation site density are two key parameters in the Dry-spot model. For the bubble departure diameter the expression by Fritz, as introduced in equation 2.31 in section 2.6.4, is used as an estimation for this parameter. The variation of the estimated bubble departure diameter with wall temperature is studied for constant conditions with inlet velocity $V = 1$ m/s, subcooling $\Delta T_{sub} = 40$ °C and bubble contact angle set to $\theta = 30$ °. The result is shown in figure 4.9, where it can be noted that the parameter decrease slightly with an increase in wall temperature. The trend of a decrease in bubble departure diameter with temperature implies that the bubbles depart earlier for an increase in wall temperature, which is as expected. Although the bubble departure diameter do not differ much with wall temperature at constant conditions, the expression include the uncertain parameter bubble contact angle, which can have a significant impact on the predictions when changed. This can be seen in figure 4.10 where predictions of the wall heat flux are presented using different values of the bubble contact angle. The value of this parameter has a large impact on the predictions of the DNB by the Dry-spot model. As the bubble contact angle is increased from 10 ° to 90 ° the DNB is predicted to occur at significantly lower wall temperatures.

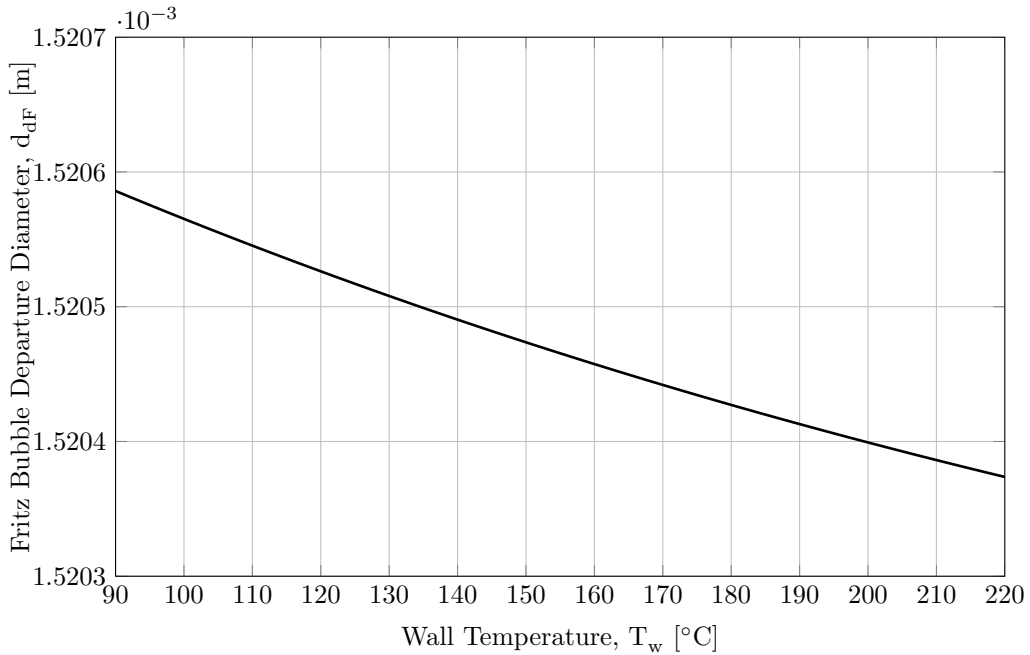


Figure 4.9: Variation of the estimated Fritz bubble departure diameter d_{dF} with wall temperature for inlet velocity $V = 1$ m/s, subcooling $\Delta T_{sub} = 40$ °C and bubble contact angle $\theta = 30$ °.

The trends of the variation of the estimated active nucleation site density with wall temperature have also been studied. In figure 4.11 the active nucleation site density is plotted against the wall temperature for constant conditions with inlet velocity $V = 1$ m/s, subcooling $\Delta T_{sub} = 40$ °C and bubble contact angle $\theta = 30$ °. The active nucleation site density is low until the wall temperature approaches approximately 170 °C where the parameter starts to increase rapidly with an increase in temperature. This is also the point where film boiling starts to be the dominant part of the heat transfer, which can be seen in figure 4.2. The effects of an increase in active nucleation sites on the surface are that more possible sites for bubbles to nucleate and grow appear, which means an increased possibility that dry-spots develop on the surface.

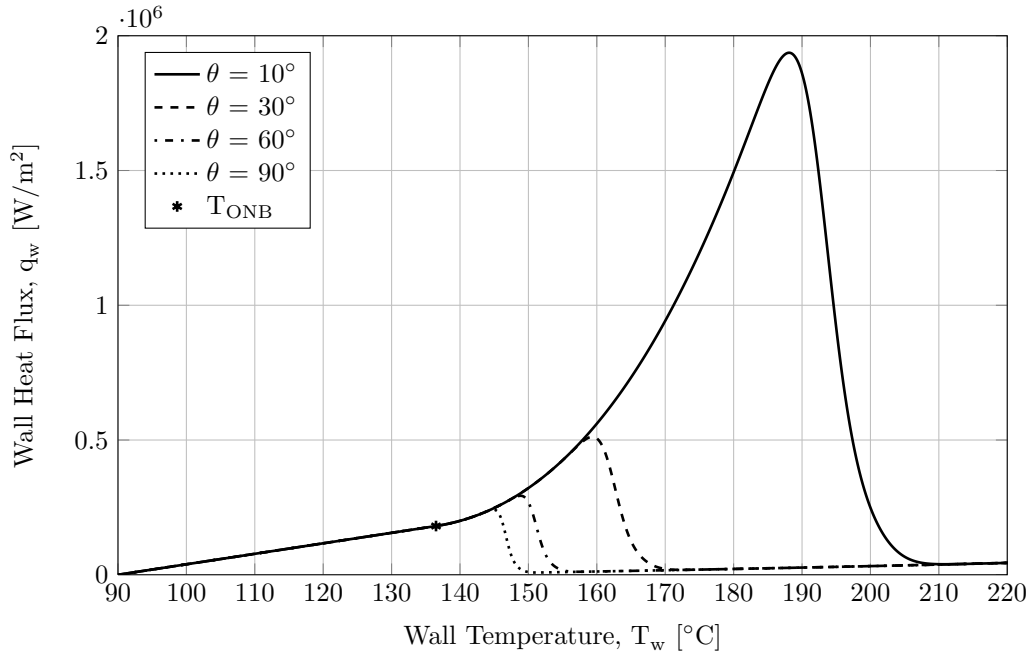


Figure 4.10: Predictions of wall heat flux using the Chen correlation together with the Dry-spot model for different values of the bubble contact angle θ . Inlet velocity $V = 1 \text{ m/s}$ and subcooling $\Delta T_{sub} = 40^\circ\text{C}$ are used.

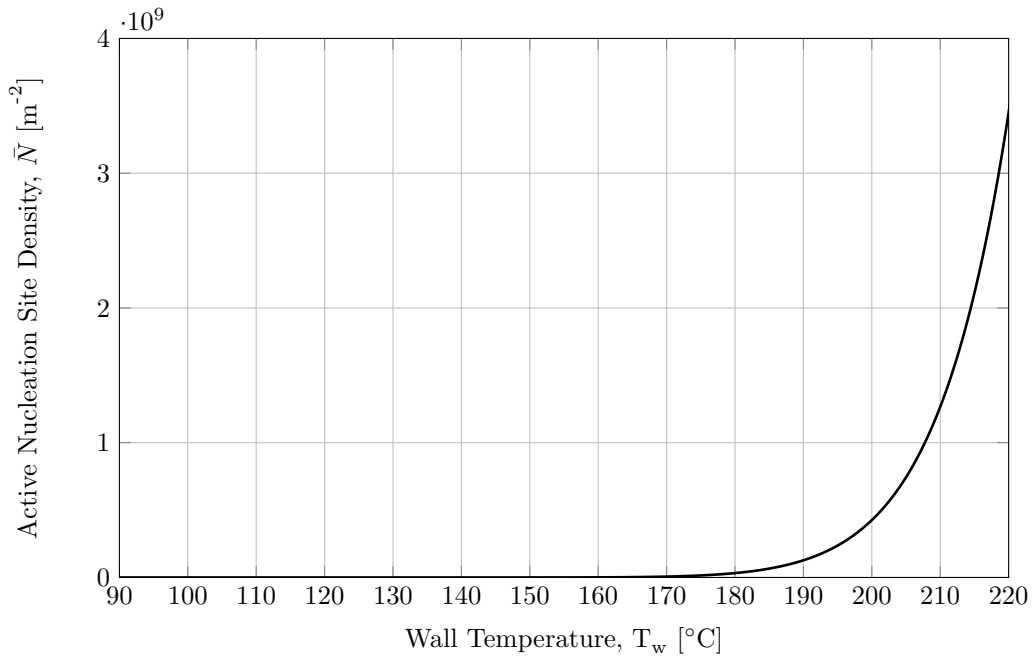


Figure 4.11: Estimated active nucleation site density \bar{N} for an inlet velocity $V = 1 \text{ m/s}$, subcooling $\Delta T_{sub} = 40^\circ\text{C}$ and bubble contact angle $\theta = 30^\circ$.

4.2 Simulations in Star-CCM+

The boiling models that are studied in Matlab have also been implemented in Star-CCM+ for a 3D analysis. Simulations are performed on two different geometries: a simplified test case geometry and an engine cooling jacket. The geometries and set-up are presented in section 3.4.2 and 3.4.3.

4.2.1 Test case

The first simulations for the test case have been run as non-conjugate heat transfer simulations without the solid structure. The simulations are performed at four different inlet velocities and a temperature boundary condition is set for the heater plate, as seen in figure 3.1a. This temperature is gradually increased to achieve boiling curves.

The impact of velocity on the ONB temperature and the suppression factor for the test case is presented in table 4.2. The trends and values are very similar to those obtained in the corresponding Matlab simulations in table 4.1, especially the ONB temperatures. The small variations might be an effect from the 3D flow. Another difference is that the built-in model for convection in Star-CCM+ is used here instead of the Dittus-Boelter correlation, but this has a minor effect as the results presented below shows.

Table 4.2: The predicted ONB temperatures and the suppression factors for different velocities. The saturation temperature of the coolant mixture is 130.7°C .

Velocity [m/s]	T_{ONB} [$^\circ\text{C}$]	S
0.25	134	0.8340
1.00	136	0.6338
3.00	139	0.4266
5.00	141	0.3331

The impact of different velocities on the heat transfer with convection and the Chen correlation applied is presented in figure 4.12.

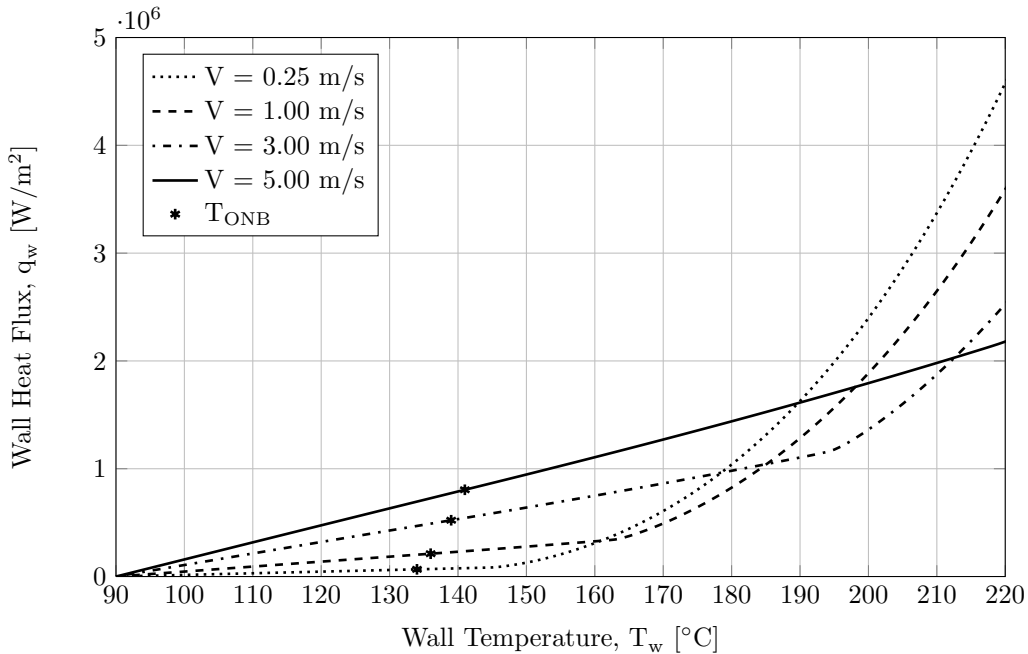


Figure 4.12: The heat transfer predictions of the Chen correlation for different velocities at subcooling $\Delta T_{\text{sub}} = 40^\circ\text{C}$.

From studying the boiling curves in the figure, it is evident that an increase in velocity also increases the convective heat transfer, similarly as in Matlab. But unlike the results obtained with Matlab, the addition to the heat flux due to nucleate boiling starts later, after the ONB has been reached, especially for higher velocities.

This behaviour is most likely due to conflicts between the built-in convection model in Star-CCM+ and the user-implemented boiling heat transfer models. To evaluate this hypothesis, the Dittus-Boelter correlation has also been implemented in Star-CCM+ and is used instead of the built-in method for convection. The results show that when using the Dittus-Boelter correlation, the heat transfer increases directly after the ONB. This is a trend that resembles the Matlab results better. The simulations with the Dittus-Boelter correlation applied are run for the velocities 0.25 and 3 m/s with also the Dry-spot model included. The results are presented in figure 4.13 and 4.14. These two figures can be compared with the results in figure 4.15 and 4.16, where the built-in convection in Star-CCM+ is used. No significant differences for the convective parts can be noted when comparing the two convection models.

For the results with velocity 0.25 m/s in figure 4.15, the delay in increased heat transfer after the ONB can clearly be seen. When applying the Dry-spot model a deviating behaviour appears after the DNB. The smooth reduction in heat transfer after the maximum heat flux that is seen in the Matlab results is here not achieved. Instead, the heat transfer levels out halfway between the maximum point and the low film boiling heat flux, but after a small increase in wall temperature it continues to decrease all the way down to the film boiling level. This behaviour is not that prominent when using the Dittus-Boelter correlation (figure 4.13) but can still be observed. The maximum achieved heat flux is somewhat higher when using the Dittus-Boelter correlation compared to when using the built-in convection in Star-CCM+. The delay in heat transfer increase after the ONB is probably one cause for this, which can be related to the uncertainty of how the built-in convection model affects the user-implemented boiling heat transfer models. By comparing the results with Matlab (figure 4.4) it can be concluded that similar values for the maximum heat flux are obtained when using the Dittus-Boelter correlation.

Considering the inlet velocity of 3 m/s similar results as described for 0.25 m/s are obtained (figure 4.14 and figure 4.16). When using the built-in convection model the delay in heat transfer increase after ONB is even larger, such that the DNB occurs before any significant contribution from the Chen correlation is obtained. The maximum heat flux observed for the Star-CCM+ and Matlab cases at 3 m/s differs slightly but can be considered to be of the same range. However, the wall temperature at maximum heat flux differs more between the cases compared to the results for an inlet velocity of 0.25 m/s.

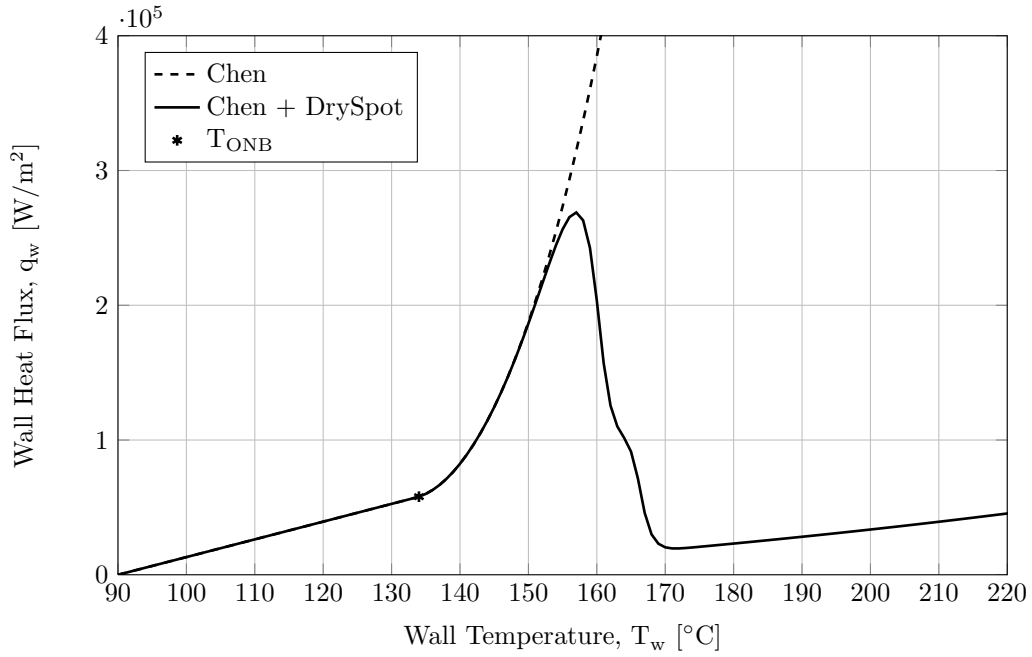


Figure 4.13: The estimated boiling curve for the test case when using the Dittus-Boelter correlation for convective heat transfer and the Chen correlation together with the Dry-spot model for the boiling heat transfer. The case is run with inlet velocity $V = 0.25$ m/s, subcooling $\Delta T_{sub} = 40$ °C and bubble contact angle $\theta = 30$ °.

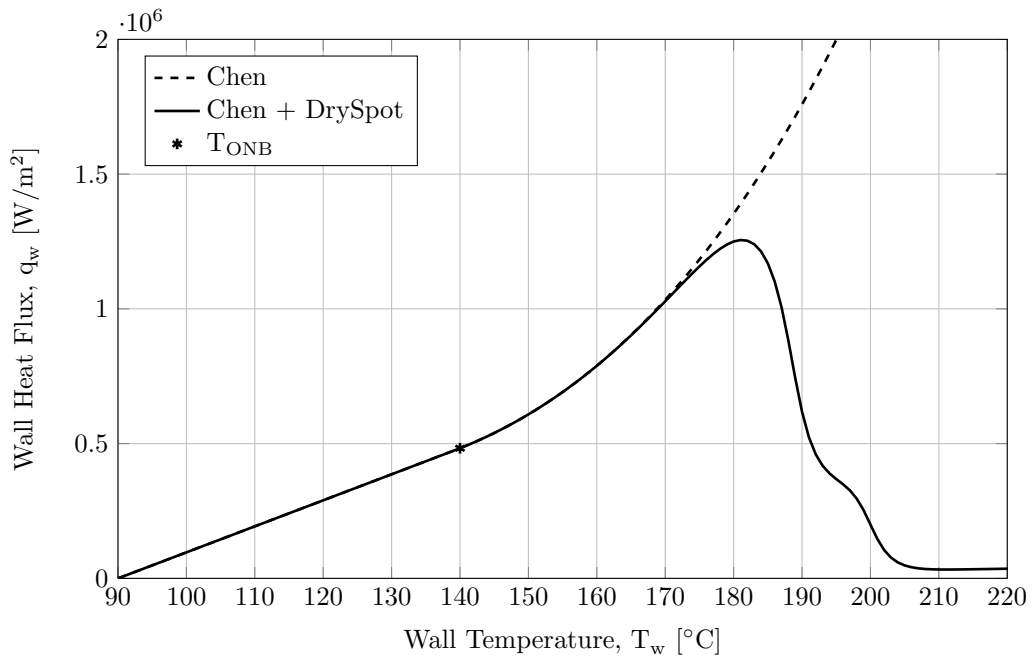


Figure 4.14: The estimated boiling curve for the test case when using the Dittus-Boelter correlation for convective heat transfer and the Chen correlation together with the Dry-spot model for the boiling heat transfer. The case is run with inlet velocity $V = 3$ m/s, subcooling $\Delta T_{sub} = 40$ °C and bubble contact angle $\theta = 30$ °.

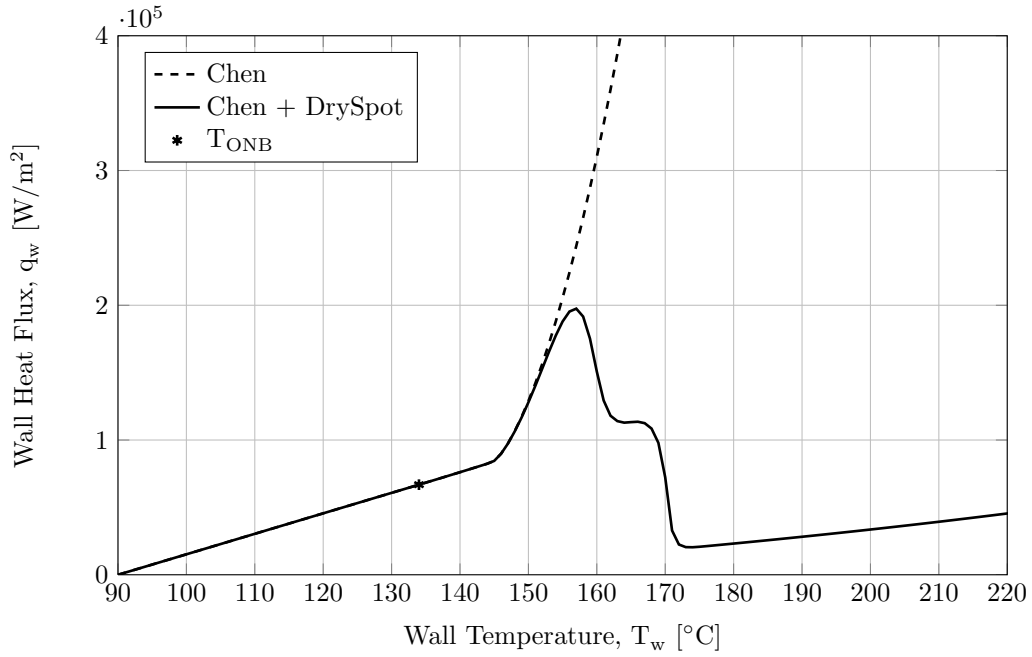


Figure 4.15: The estimated boiling curve for the test case when using the built-in model for convective heat transfer and the Chen correlation together with the Dry-spot model for the boiling heat transfer. The case is run with inlet velocity $V = 0.25$ m/s, subcooling $\Delta T_{sub} = 40$ °C and bubble contact angle $\theta = 30$ °.

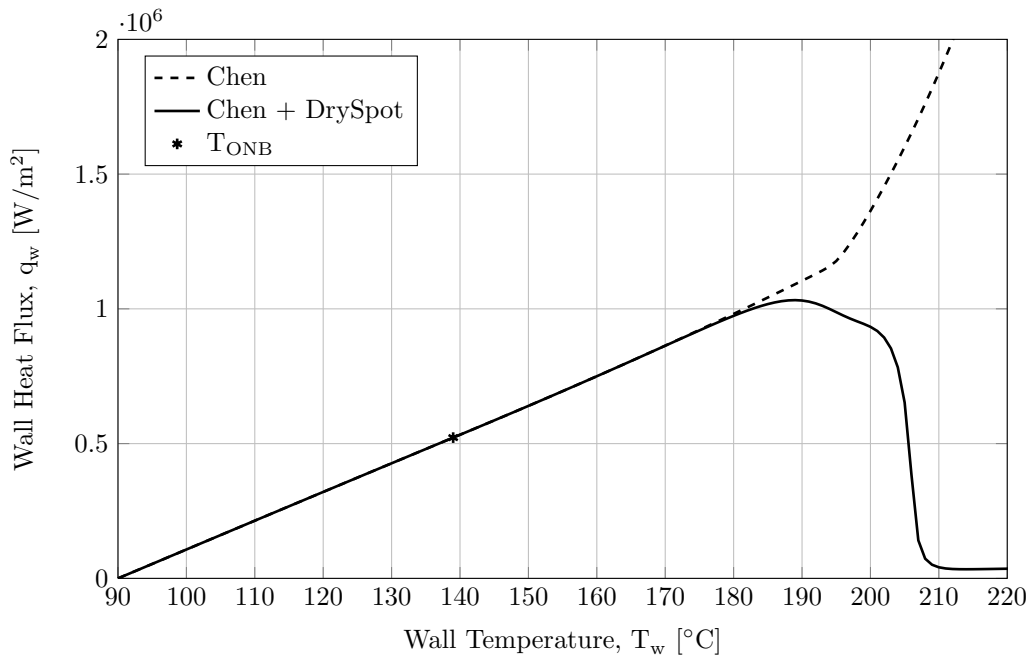


Figure 4.16: The estimated boiling curve for the test case when using the built-in model for convective heat transfer and the Chen correlation together with the Dry-spot model for the boiling heat transfer. The case is run with inlet velocity $V = 3$ m/s, subcooling $\Delta T_{sub} = 40$ °C and bubble contact angle $\theta = 30$ °.

Conjugate heat transfer simulations

Conjugate heat transfer simulations have been performed for the test case with five different inlet velocities to evaluate the behaviour of the ONB scalar indicator. Only the built-in convective heat transfer model in Star-CCM+ is used for these cases. A fixed temperature of 170°C is set on the outer bottom wall of the solid part. The heat is transported by conduction through the solid domain to the solid-fluid interfaces where boiling can be present. The impact of velocity on the ONB scalar indicator is presented in figure 4.17. The steps in velocity have been chosen such that the effects are captured. The figure shows the fluid domain of the test section for five different velocities and the areas where boiling is predicted are colored. From the figure it can be concluded that the suppression of nucleate boiling is enhanced with an increase in velocity.

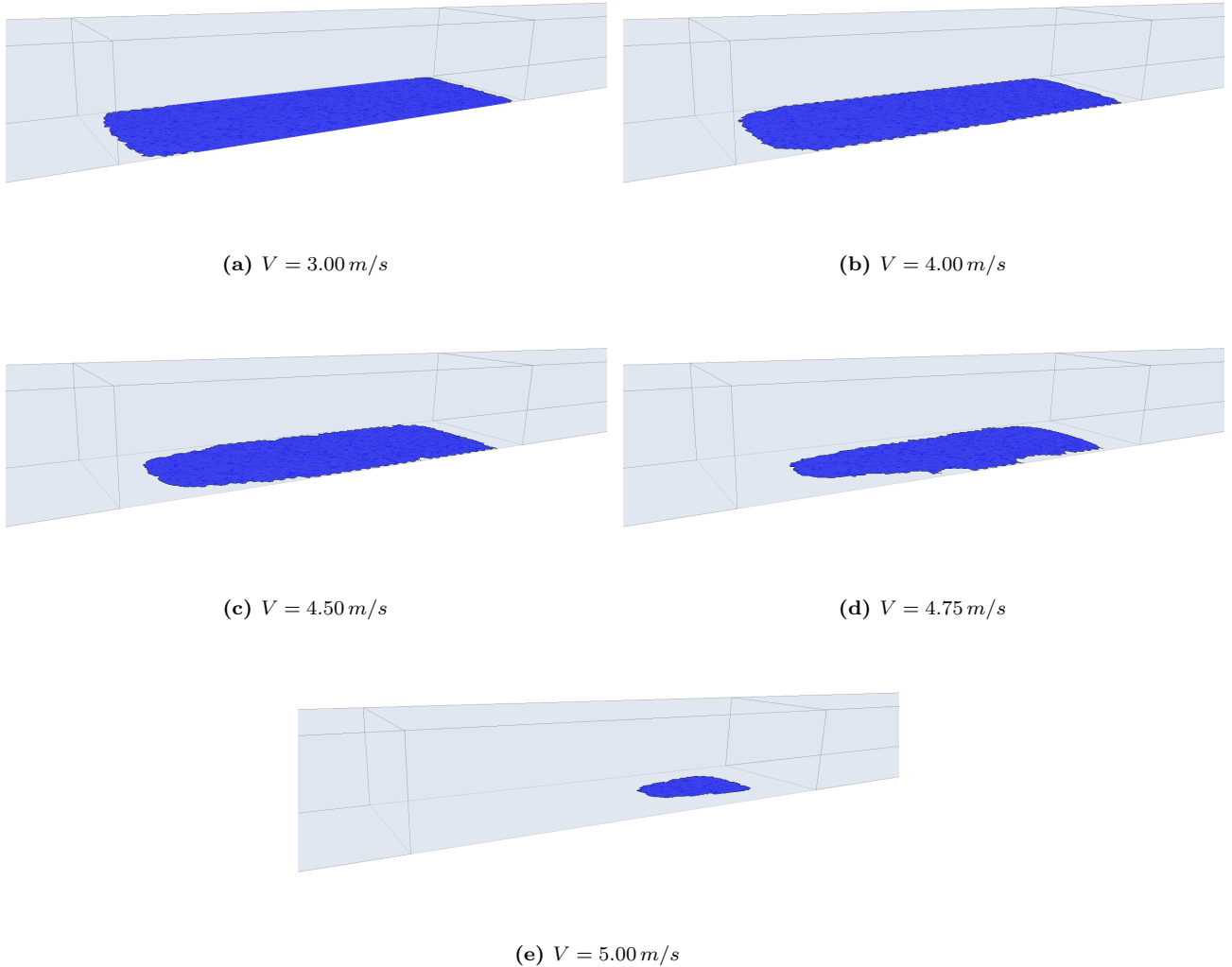


Figure 4.17: The impact of inlet velocity on the predictions of ONB for the test case with subcooling $\Delta T_{sub} = 40^{\circ}\text{C}$.

Conjugate heat transfer simulations have also been performed for the test case with the Chen correlation applied to estimate the temperature distribution. Attempts have been made to include the Dry-spot model in the simulations, but without good results. Stability issues occur when including the Dry-spot model in the boiling heat transfer calculations. The simulations with the Dry-spot model work for lower temperatures but when the temperatures are increased such that film boiling is developed, convergence issues appear. However, it is possible to compute the parameters in the Dry-spot model to obtain predictions of the boiling scalar indicator, as long as the model is not used for the boiling heat transfer calculations.

Limitation of the nucleate boiling heat flux

To investigate the effects of an unlimited maximum fluid temperature for the non-conjugate heat transfer simulations, case 7 and 8 have been performed according to table 3.4. The boiling curves when using the Chen correlation with and without a limited maximum temperature are compared in figure 4.18 for the inlet velocity of 3 m/s. As expected when the fluid temperatures are unlimited, the near wall fluid temperatures become larger than the wall temperatures for higher wall temperatures. But when studying the boundary heat flux in the figure, it is seen that the contribution from the Chen correlation is small and the boiling curve more or less resembles the curve when only using convective heat transfer. When the temperatures are limited, the addition from the Chen correlation to the wall heat flux is increased after the ONB but delayed as previously noted. This has not been fully understood during this thesis, but it is an important aspect that needs to be investigated. It is likely a matter of how the software handles the user-implemented models in combination with the built-in models.

For the conjugate heat transfer simulations, two different approaches have been tested regarding the SF factor as discussed in section 3.4.1. When setting the factor as 0 or 1 the simulations become unstable and no converged solution is obtained. Therefore, the extended expression for the SF factor, where it more smoothly takes a value between 0 and 1, is used in all conjugate heat transfer simulations. This results in increased stability.

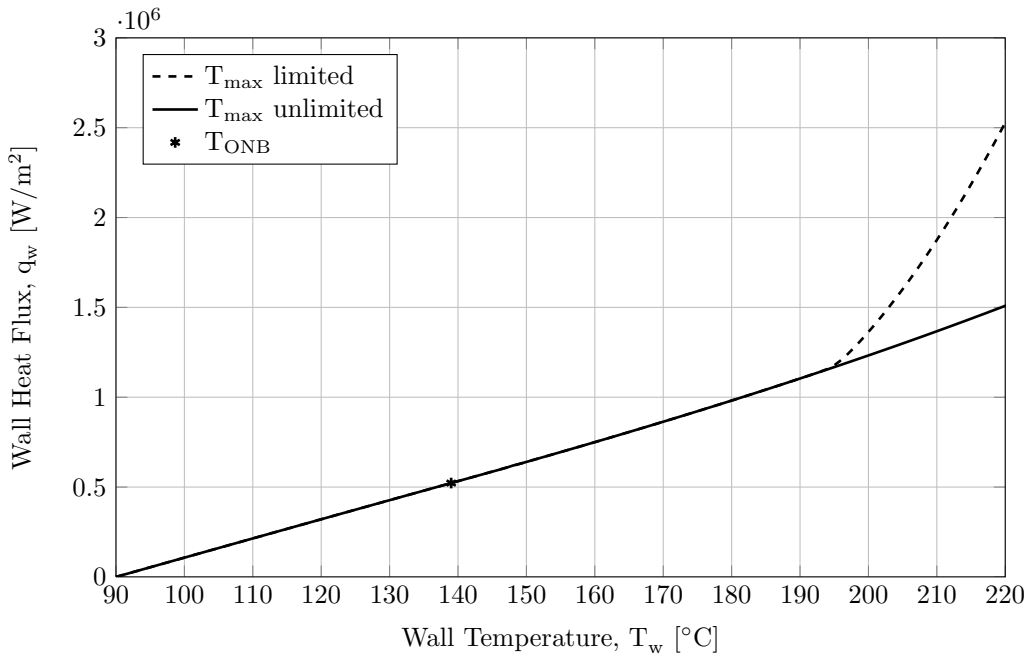


Figure 4.18: A comparison between the estimated boiling curves with and without the maximum fluid temperature limited when using the Chen correlation. The cases are run with inlet velocity $V=3$ m/s and subcooling $\Delta T_{\text{sub}}=40$ °C.

4.2.2 Engine cooling jacket

The boiling models and scalar indicators have also been applied to an engine cooling jacket at operational conditions as described in section 3.4.3. Three different simulation cases with different activated models to describe the heat transfer have been aimed to be run for the geometry: one simulation using only convective heat transfer, one with the addition of the Chen correlation to describe the effects from nucleate boiling and finally one where also the Dry-spot model is applied. The ONB scalar indicator is applied for all simulations and the boiling scalar indicator is used in the simulations with the Chen correlation. The results from the simulations are presented in the following sections.

ONB scalar indicator

The ONB scalar indicator makes it possible to predict where in the geometry nucleate boiling has started to occur. The scalar indicator takes the value of 1 if boiling is present and 0 otherwise. Figure 4.19 presents the predictions of the ONB scalar indicator for the fluid-solid interfaces of the engine cooling jacket. It is here seen that boiling is predicted in several areas in the geometry. Most of the boiling is predicted in the cylinder head but boiling is also predicted in some areas in the cylinder block.

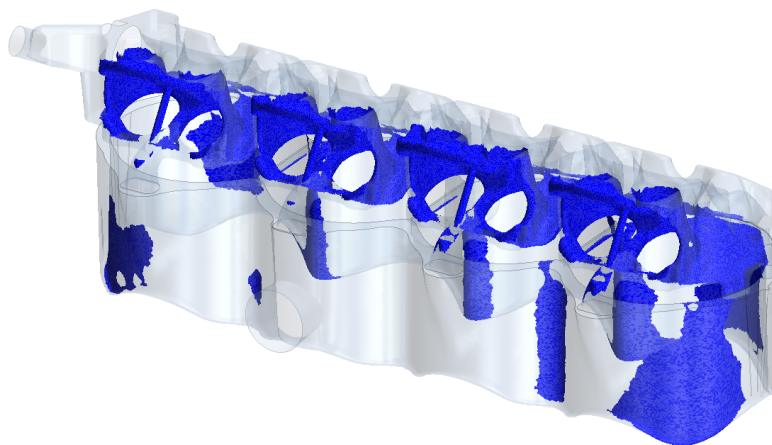


Figure 4.19: *The prediction of ONB in the engine cooling jacket.*

Temperature distributions

The simulations of the cooling jacket with the built-in convective heat transfer model and the Chen correlation have been run without any implications. The wall temperature distribution of the cooling jacket when only the built-in convective heat transfer model in Star-CCM+ is used can be seen in figure 4.20. When the Chen correlation is applied the temperature distribution in figure 4.21 is obtained. By comparing the distributions it can be seen that the temperature is decreased in some areas when the Chen correlation is applied because of the increase in wall heat transfer due to the nucleate boiling. The temperature distributions of the cylinder head is studied in more detail in figure 4.22 where only convection is active and in figure 4.23 where also the Chen correlation is applied. Here the differences in temperature can be seen in the upper parts of the figures. By comparing the changes in temperature distribution with the predictions of ONB in figure 4.19 it is concluded that the temperature differs in the areas where ONB is predicted.

If the boiling that occurs is within the nucleate boiling regime, the Chen correlation can be applied as it is. But if film boiling is developed, the Chen correlation is used in areas outside of its range of applicability and the addition of the Dry-spot model is therefore needed to better describe the heat transfer. However, when activating the Dry-spot model the simulations become unstable and convergence is not reached. It is only possible to use the Dry-spot model when the heat transfer coefficients in the solid part are significantly decreased such that the wall temperatures of the domain are lowered. But the simulations do not converge when the coefficients are raised again and therefore, no results with the Dry-spot model activated for the heat transfer have been achieved for the engine cooling jacket.

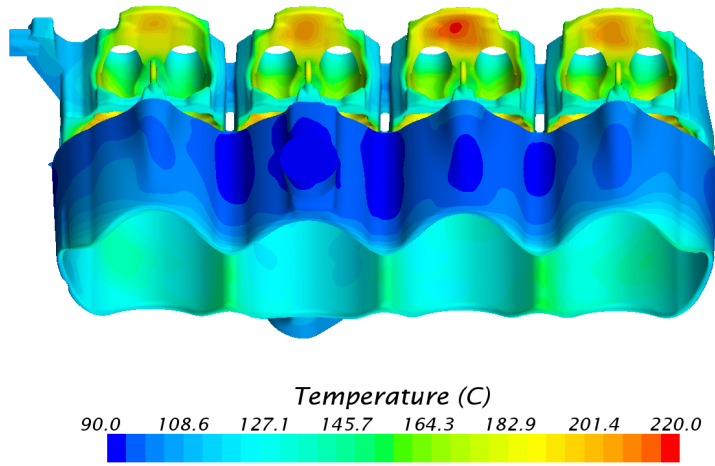


Figure 4.20: Temperature distribution on the walls of the cooling jacket for simulations with the built-in convective heat transfer model in Star-CCM+.

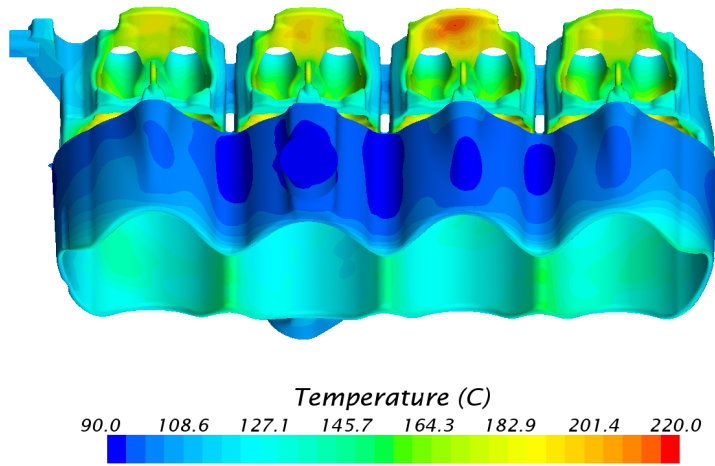


Figure 4.21: Temperature distribution on the walls of the cooling jacket for simulations with the addition of the Chen correlation.

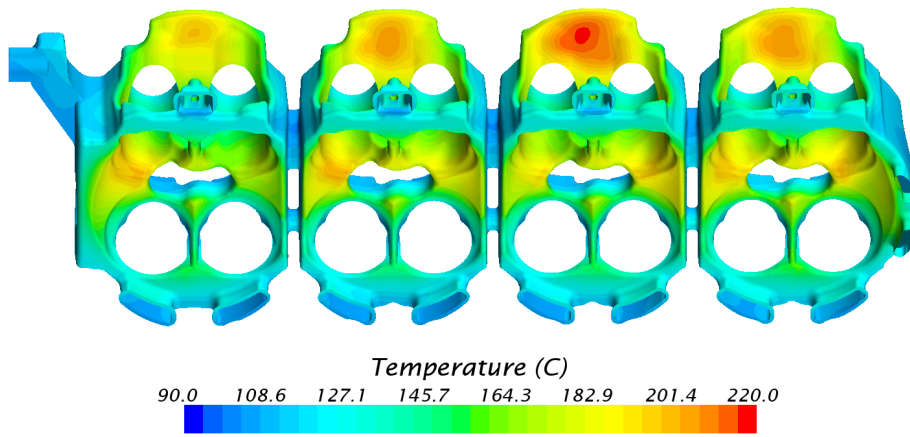


Figure 4.22: Temperature distribution on the walls of the cylinder head from below, for simulations with the built-in convective heat transfer model in Star-CCM+.

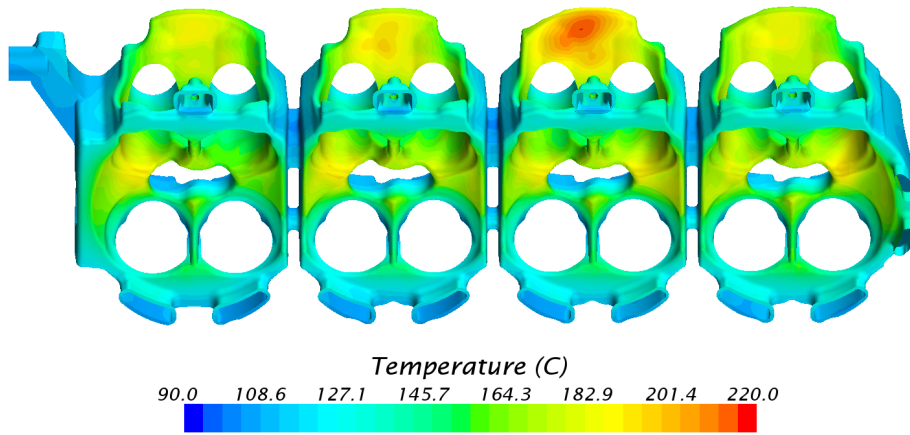


Figure 4.23: Temperature distribution on the walls of the cylinder head from below, for simulations with the addition of the Chen correlation.

Boiling scalar indicator

Although no converged solution have been achieved with the Dry-spot model activated in the heat transfer predictions, it is possible to compute its parts to be able to estimate if DNB has started. In this way, the boiling scalar indicator is computed and plotted on the geometry to predict if film boiling is present. The results of the predictions when applying the boiling scalar indicator to the engine cooling jacket is seen in figure 4.24 for the whole domain and in figure 4.25 for the cylinder head from below. The predictions of ONB is colored in blue and the parts where DNB has been reached are indicated in red. By studying the figures it is seen that film boiling is predicted on some areas in the cylinder block but for the cylinder head film boiling is considerably more spread. In these areas the heat transfer should be significantly decreased with the effect of an increase in temperature compared to the temperatures in figure 4.20-4.23. In the areas indicated in blue, the heat transfer is instead enhanced due to the nucleate boiling heat transfer which improves the cooling effect. This shows the importance of including both nucleate and film boiling heat transfer when designing an engine cooling jacket.

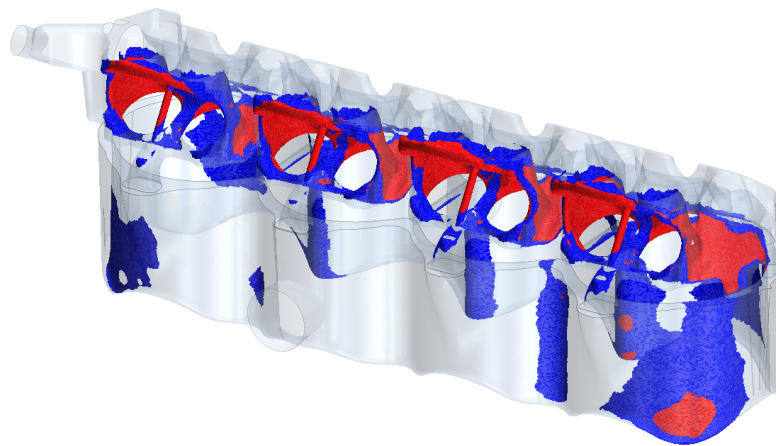


Figure 4.24: *The boiling scalar indicator applied to the cooling jacket (Blue = ONB and Red = DNB).*

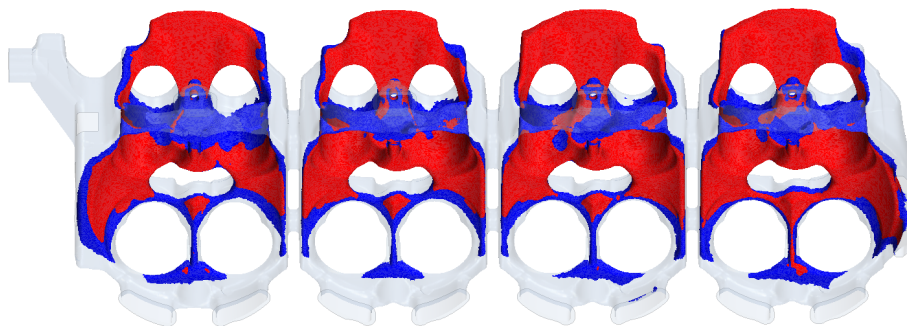


Figure 4.25: *The boiling scalar indicator on the cylinder head from below (Blue = ONB and Red = DNB).*

5 Discussion

One of the purposes with this master thesis is to investigate the possibilities of predicting the presence of boiling. As the results have shown, this can be done with the ONB scalar indicator based on the condition of Hsu. Some advantages are the low demand for computational power and the good compatibility with the standard CAE analyses performed at Volvo Cars today. The condition of Hsu has also in previous work been proven to give reasonable estimates of the ONB and has been used extensively in practical applications [6]. The results from the simulations show that the ONB is predicted to occur in a range of approximately 0-10 degrees above the saturation temperature of the liquid depending on flow conditions. The ONB occurs at a higher wall temperature with an increased velocity as expected and the predictions in Matlab and the test case in Star-CCM+ give similar results for each inlet velocity. This is the case when both the built-in model in Star-CCM+ and the Dittus-Boelter correlation for the convective heat transfer are used. However, the condition assumes a static bubble contact angle of 90° which might not be the case for the engine cooling jacket. If the angle is smaller the ONB will occur at a higher wall temperature and the boiling process will be delayed. On the other hand, if the angle is larger than 90° the boiling process will be initiated at a lower wall temperature and the ONB condition of Hsu will underestimate the ONB. The condition also assumes a wide range of active nucleation cavities of all sizes. If this is not the case the boiling might be initiated at a higher wall temperature and the condition of Hsu will overestimate the ONB.

The Chen correlation has been implemented and run for all simulation cases and it is able to describe the trends of the heat transfer in the nucleate boiling regime and shows a rapid increase in heat transfer after the point of ONB. The results when applied to the cooling jacket shows a decrease in wall temperature in the areas where ONB is predicted compared to the convective heat transfer simulations, which is as expected. The correlation was originally developed for very specific conditions but has proven to give reasonable results even outside these conditions. The correlation is here mainly chosen due to its previous use on engine cooling systems where it captured the trends of the heat transfer. A drawback of the model is the use of bulk flow properties, which are hard to extract for a complex geometry such as the engine cooling jacket. In this thesis the properties are taken as volume averages over the entire domain. This assumption can be appropriate for most parts of the engine cooling jacket since the temperature differences between the inlet and outlets are small, in the range of approximately 2-6 °C. However, the bulk temperatures might locally be increased in the smallest passages, giving different properties. Another limitation with the correlation is the dependency on the hydraulic diameter which varies significantly within an engine cooling jacket and can be hard to compute due to the shapes of the channels. The hydraulic diameter is used when computing the suppression factor S , which has a large impact on the heat transfer in the nucleate boiling regime as can be seen in the results (figure 4.5 and 4.6). For this work the hydraulic diameter is assumed to have a constant value of 0.01 m and is based on measurements in the geometry. No further investigation of the effects of this parameter could be performed during the time of this thesis but further evaluation is needed.

Another subject for discussion is how the built-in method for convection in Star-CCM+ affects the implementation. As can be seen from the results of the test case in figure 4.15 and 4.16, the addition to the heat transfer from the Chen correlation is delayed even though the point of ONB has been reached. This indicates that there is a conflict between the built-in convection model and the implemented Chen correlation, where the built-in convection model compensates in some way for the addition to the heat flux from the Chen correlation. This is not the case when instead using the Dittus-Boelter correlation in the implementation as can be seen in figure 4.13 and 4.14, where the boiling curves increase directly after the ONB. It is therefore not certain that the User Defined Wall Heat Flux Specification is a suitable method to use for this purpose. Further information from the software developer might contribute to solve the problem, but other methods to include the heat transfer addition from the Chen correlation should be investigated otherwise. The fact that the temperatures in the near wall cells need to be limited to avoid non-physical fluid temperatures can possibly explain this more. When the temperatures are not limited, the boiling curve seems to be similar to the curve when only convection is considered (figure 4.18), but with the effect that the temperatures in the near wall cells become higher than the wall temperature. This indicates that the addition from the Chen correlation is added to the fluid without increasing the boundary heat flux. When the temperatures are limited another behaviour of the boiling curve is achieved as discussed above, where the addition from the Chen correlation increases the boundary heat flux after the point of ONB, but somewhat delayed.

The Dry-spot model is used in the simulations to set an upper limit for when the Chen correlation is valid and to describe the heat transfer better at high wall temperatures. From studying the Matlab results in figure 4.2, it can be seen that the Dry-spot model captures the trends of the DNB and the subsequent rapid decrease in heat transfer. When the model is applied to the test case in Star-CCM+ a similar behaviour is observed when the Dittus-Boelter correlation is used for the convective heat transfer, as presented in figure 4.13 and 4.14. When instead using the built-in convection model in Star-CCM+, the previously stated conflict between the user-implemented correlation and the built-in model is evident when also using the Dry-spot model (figure 4.15 and 4.16). The delay in heat transfer increase from the Chen correlation remains, which has the impact that the DNB starts before any significant addition to the heat transfer is seen for the velocity of 3 m/s. It should be noted that this is not a direct consequence of the Dry-spot model. Apart from this, the smooth decrease in heat transfer after the maximum heat flux that is obtained in Matlab is not achieved in Star-CCM+. Instead, the decrease in heat flux levels out before starting to decrease again towards the low film boiling heat flux. This is also seen when using the Dittus-Boelter correlation, but appears less significant. Hence, this is probably not a consequence of the conflict mentioned above, but the cause has not been understood during the time of this thesis.

Two important parameters in the Dry-spot model are the bubble departure diameter and the active nucleation site density. What models or correlations that are used to estimate these parameters can have large impact on the behaviour of the Dry-spot model. An important parameter in the expression for the bubble departure diameter used in this thesis is the bubble contact angle and since the expression used for the active nucleation site density includes the bubble departure diameter, this expression is also affected by the bubble contact angle. The impact of the bubble contact angle on the boiling curve is shown in figure 4.10 where it is seen that the DNB occurs at lower wall temperatures for an increased value of the angle. The bubble contact angle is hard to estimate and will most likely vary in the engine cooling jacket, which is not considered in the simulations in this thesis. Furthermore, the phenomena of DNB and CHF are still not completely understood by researchers and the models, like the Dry-spot model, are mainly based on postulated mechanisms that make it hard to estimate the accuracy before a validation has been performed for the specific case. This is also why the Dry-spot model here is used mainly as an upper limit for the Chen correlation.

Regarding the use of the Dry-spot model for the conjugate heat transfer simulations it is possible to run the Dry-spot model on the side, not activated for the heat transfer predictions, to be able to compute the boiling scalar indicator. But when the Dry-spot model is activated for the heat transfer predictions, convergence issues occur and no results have been obtained neither for the test case or for the engine cooling jacket. The convergence issues appear at rather high wall temperatures where film boiling most likely is present. By investigating the simulations in detail, it is concluded that the model seems to work for temperatures just in the beginning of the DNB but that the simulations diverge for slightly higher temperatures. This indicates that the cause might be a sudden decrease in heat transfer as film boiling starts to develop and is therefore considered a numerical issue. Different methods to under-relaxating the boiling heat flux have been tested without success.

When using the Chen correlation for the engine cooling jacket the wall temperatures decrease in the areas where boiling is predicted by the ONB condition, compared to the simulations with only convective heat transfer taken into account. The trends are as expected, but the conflict between the implemented correlation and the built-in method in Star-CCM+ infers that further improvements are needed before a validation is performed. The boiling scalar indicator has been computed for the engine cooling jacket and shows on some areas with film boiling. The method of the indicator works good and the predictions are reasonable, but since it is dependent on both the Chen correlation and the Dry-spot model the accuracy of the values is questionable until the models are improved and validated by experiments.

6 Conclusions

A method to model subcooled nucleate flow boiling using 1D models and correlations has been developed in this study as a first step towards including boiling in the standard CAE analysis at Volvo Cars. The method consists of an ONB condition used to predict the presence of boiling, the Chen correlation to estimate the heat transfer in the nucleate boiling regime and the Dry-spot model to put an upper limit to the heat flux and to estimate when the Chen correlation is no longer valid. The use of the Chen correlation and the Dry-spot model emphasize some advantages and limitations regarding the modeling and implementation process in Star-CCM+.

An ONB scalar indicator has successfully been implemented and predicts boiling in some areas in the engine cooling jacket, mainly in the cylinder head around the exhaust ports. The Chen correlation has been implemented and results in a rapid increase in heat transfer after the ONB, as expected, but somewhat delayed when using the built-in convection model in Star-CCM+. The latter is probably due to a conflict between the built-in model and the Chen correlation implemented through the User Defined Wall Heat Flux Specification in Star-CCM+. The Chen correlation applied to the engine cooling jacket results in lowered temperatures in those areas where ONB is predicted.

The use of the Dry-spot model in combination with the Chen correlation shows on the right trends when evaluating the method in Matlab and for non-conjugate heat transfer simulations in Star-CCM+. But when applied to the conjugate heat transfer simulations, convergence issues appear and no results have been obtained. Nonetheless, it is possible to run the Dry-spot model on the side, not active in the heat transfer predictions, to be able to compute the boiling scalar indicator which indicates that film boiling is present in some areas in the engine cooling jacket.

A parameter study has been performed in Matlab to investigate how some parameters influence the heat transfer. The study shows that the flow velocity has a large impact on the heat transfer predictions when including both the Chen correlation and the Dry-spot model. An increased velocity significantly enhances the convective part of the heat transfer but has less impact on the nucleate boiling part that is slightly suppressed. The effects of the suppression factor have also been investigated and show on great importance for the nucleate boiling part of the heat transfer predictions. The DNB is initiated earlier with a higher suppression factor which means that film boiling occurs at lower wall temperatures. The value of the bubble contact angle in the expression used to estimate the bubble departure diameter in the Dry-spot model has a large influence on the predictions of the DNB. For a low bubble contact angle the bubbles depart later from the surface and the DNB occurs at a higher wall temperature. The parameter study also includes the degree of subcooling, which affects the Chen correlation mostly in the beginning of the nucleate boiling regime since the subcooling is only included in the convective part of the correlation.

Further improvements to the presented issues are needed before the models are ready to be included in the standard CAE analysis performed at Volvo Cars. It is also important that the models are validated through experiments to be able to determine the accuracy.

7 Further work

Using the Chen correlation is a first step in developing a 1D boiling model but there is room for further improvements in some areas, especially regarding the geometry dependency of the correlation. For instance, it would be interesting to evaluate and compare the BDL-model which is a further modification of the Chen correlation, aimed at making the model less dependent on geometry through expressing the suppression factor differently. Another area of improvement is to investigate the conflict between the implementation of the Chen correlation and the built-in model for convection in Star-CCM+. More information is needed about the User Defined Wall Heat Flux Specification in the software and other implementation possibilities can also be investigated. This should be a priority for further work.

It is also of importance to stabilize the Dry-spot model when applied to conjugate heat transfer simulations in order to use it for the heat transfer predictions. One possibility is to continue the work on under-relaxation of the boiling heat flux and stepwise increase the heat transfer coefficients that are specified in the solid structure.

In this work the ONB condition of Hsu has been used to predict the presence of boiling. The condition has proven to give reasonable estimations of the ONB in practical applications but there are also other conditions available in the literature that would be interesting to study and compare.

Before including any of these models in real case analyses, the predictions need to be validated with experiments to determine the accuracy. The experimental results can also be used to tune in the boiling models. The design of the experiments has to be defined and important test parameters need to be identified. It is also important to investigate experimentally how much vapor that is present in the system to be able to verify the assumption of subcooled flow boiling. If a large amount of vapor is generated, a multiphase approach might be necessary to better describe the interactions between the gas and liquid phases.

References

- [1] J. C. Chen. “Correlation for Boiling Heat Transfer to Saturated Fluids in Convective Flow”. In: *Industrial and Engineering Chemistry, Process Design and Development* 5.3 (1966), pp. 322–329.
- [2] J. G. Collier and J. R. Thome. *Convective Boiling and Condensation*. 3rd ed. Oxford: Clarendon Press, 1994. ISBN: 0-19-856282-9.
- [3] S. J. Ha and H. C. No. “A Dry-Spot Model of Critical Heat Flux in Pool and Forced Convection Boiling”. In: *International Journal of Heat and Mass Transfer* 41.2 (1998), pp. 303–311.
- [4] S. J. Ha and H. C. No. “A Dry-Spot Model for Transition Boiling Heat Transfer in Pool Boiling”. In: *International Journal of Heat and Mass Transfer* 41 (1998), pp. 3771–3779.
- [5] S. J. Ha and H. C. No. “A Dry-Spot Model of Critical Heat Flux Applicable to Both Pool Boiling and Subcooled Forced Convection Boiling”. In: *International Journal of Heat and Mass Transfer* 43 (2000), pp. 241–250.
- [6] C. T. Crowe. *Multiphase Flow Handbook*. Boca Raton, FL: CRC Taylor & Francis, 2006. ISBN: 978-0-8493-1280-9.
- [7] V. K. Dhir. “Boiling Heat Transfer”. In: *Annual Review of Fluid Mechanics* 30 (1998), pp. 365–401.
- [8] K. Robinson. “IC Engine Heat Transfer Studies”. PhD thesis. University of Bath, 2001.
- [9] R. Stone. *Introduction to internal combustion engines*. 4th ed. Palgrave Macmillan, 2012. ISBN: 978-0-230-57663-6.
- [10] S. G. Kandlikar. “Critical Heat Flux in Subcooled Flow Boiling - An Assessment of Current Understanding and Future Directions for Research”. In: *Multiphase Science and Technology* 13.3 (2001), pp. 207–232.
- [11] G. F. Hewitt. “Boiling”. In: ed. by W. M. Rohsenow, J. P. Hartnett, and Y. I. Cho. 3rd ed. Handbook of Heat Transfer. McGraw-Hill, 1998.
- [12] G. R. Warrier and V. K. Dhir. “Heat Transfer and Wall Heat Flux Partitioning During Subcooled Flow Nucleate Boiling - A Review”. In: *Journal of Heat Transfer* 128 (2006), pp. 1243–1256.
- [13] H. Puneekar and S. Das. *Numerical Simulation of Subcooled Nucleate Boiling in Cooling Jacket of IC Engine*. Ansys Inc., SAE International, 2013.
- [14] T. Bo. *CFD Homogeneous Mixing Flow Modelling to Simulate Subcooled Nucleate Boiling Flow*. SAE International, 2004.
- [15] V. K. Dhir. “Mechanistic Prediction of Nucleate Boiling Heat Transfer - Achievable or a Hopeless Task?”. In: *Journal of Heat Transfer* 128.1 (2006), pp. 1–12.
- [16] W. M. Rohsenow. “A method of correlating heat transfer data for surface boiling of liquids”. In: *Trans. ASME* 74 (1952), 969–976.
- [17] M. Cardone et al. *A Model for Application of Chen’s Boiling Correlation to a Standard Engine Cooling System*. SAE International, 2008.
- [18] H. S. Lee. *Heat Transfer Predictions using the Chen Correlation on Subcooled Flow Boiling in a Standard IC Engine*. SAE International, 2009.
- [19] N. A. F. Campbell et al. *Predictions for Nucleate Boiling - Results From a Thermal Bench Marking Exercise Under Low Flow Conditions*. SAE International, 2002.
- [20] F. Dong et al. *Numerical Simulation of Boiling Heat Transfer in Water Jacket of DI Engine*. SAE International, 2010.
- [21] A. E. Bergles and W. M. Rohsenow. “The Determination of Forced-Convection Surface-Boiling Heat Transfer”. In: *Journal of Heat Transfer* 86.3 (1964), pp. 365–372.
- [22] H. Steiner, A. Kobor, and L. Gebhard. “A Wall Heat Transfer Model for Subcooled Boiling Flow”. In: *International Journal of Heat and Mass Transfer* 48 (2005), pp. 4161–4173.
- [23] J. R. Welty et al. *Fundamentals of Momentum, Heat, and Mass Transfer*. 5th ed. United States of America: John Wiley & Sons, Inc., 2007. ISBN: 978-0470128688.
- [24] F. M. White. *Fluid Mechanics*. 7th ed. Singapore: McGraw-Hill, 2011. ISBN: 978-007-131121-2.
- [25] CD-Adapco. *User Guide: STAR-CCM+ Version 8.06*. 2013.
- [26] Y. Y. Hsu. “On the Size Range of Active Nucleation Cavities on a Heating Surface”. In: *Journal of Heat Transfer* 83.3 (1962), pp. 207–213.
- [27] N. Basu, G. R. Warrier, and V. K. Dhir. “Onset of Nucleate Boiling and Active Nucleation Site Density During Subcooled Flow Boiling”. In: *Journal of Heat Transfer* 124.4 (2002), pp. 717–728.
- [28] H. K. Forster and N. Zuber. “Dynamics of Vapour Bubbles and Boiling Heat Transfer”. In: *AIChE* 1.4 (1955), pp. 531–535.

- [29] S. G. Kandlikar. *Handbook of Phase Change: Boiling and Condensation*. Taylor & Francis Ltd, 1999. ISBN: 9781560326342.
- [30] G. Kocamustafaogullari and M. Ishii. “Interfacial Area and Nucleation Site Density in Boiling Systems”. In: *International Journal of Heat and Mass Transfer* 26.9 (1983), pp. 1377–1387.
- [31] T. D. Bui and V. K. Dhir. “Film Boiling Heat Transfer on an Isothermal Vertical Surface”. In: *Journal of Heat Transfer* 107.4 (1985), pp. 764–771.
- [32] S. Mörtstedt and G. Hellsten. *Data och diagram: Energi- och kemitekniska tabeller*. 7th ed. Liber AB, 2010. ISBN: 978-91-47-00805-6.
- [33] BASF. *Technical Information: Glythermin NF*. TI/EVO 1023 e. 2007.
- [34] Knovel Corporation. *Knovel online engineering database*. 2014. URL: <http://why.knovel.com>.
- [35] M. Holmgren. *XSteam: Water and steam properties according to IAPWS IF-97*. URL: <http://xsteam.sourceforge.net>.